Power spectra of black holes and neutron stars as a probe of hydrodynamical structure of the source. Diffusion theory and its application to Cyg X-1 and Cyg X-2 X-ray observations

Lev Titarchuk (GMU/NRL/GSFC/University of Ferrara),
Nikolai Shaposhnikov (GSFC), and Vadim Aref'ev (IKI)

February, 22 2007, Milano, Italy

Transition Layer (Compton Cloud) Model of Accretion Process Surrounding a Compact Object

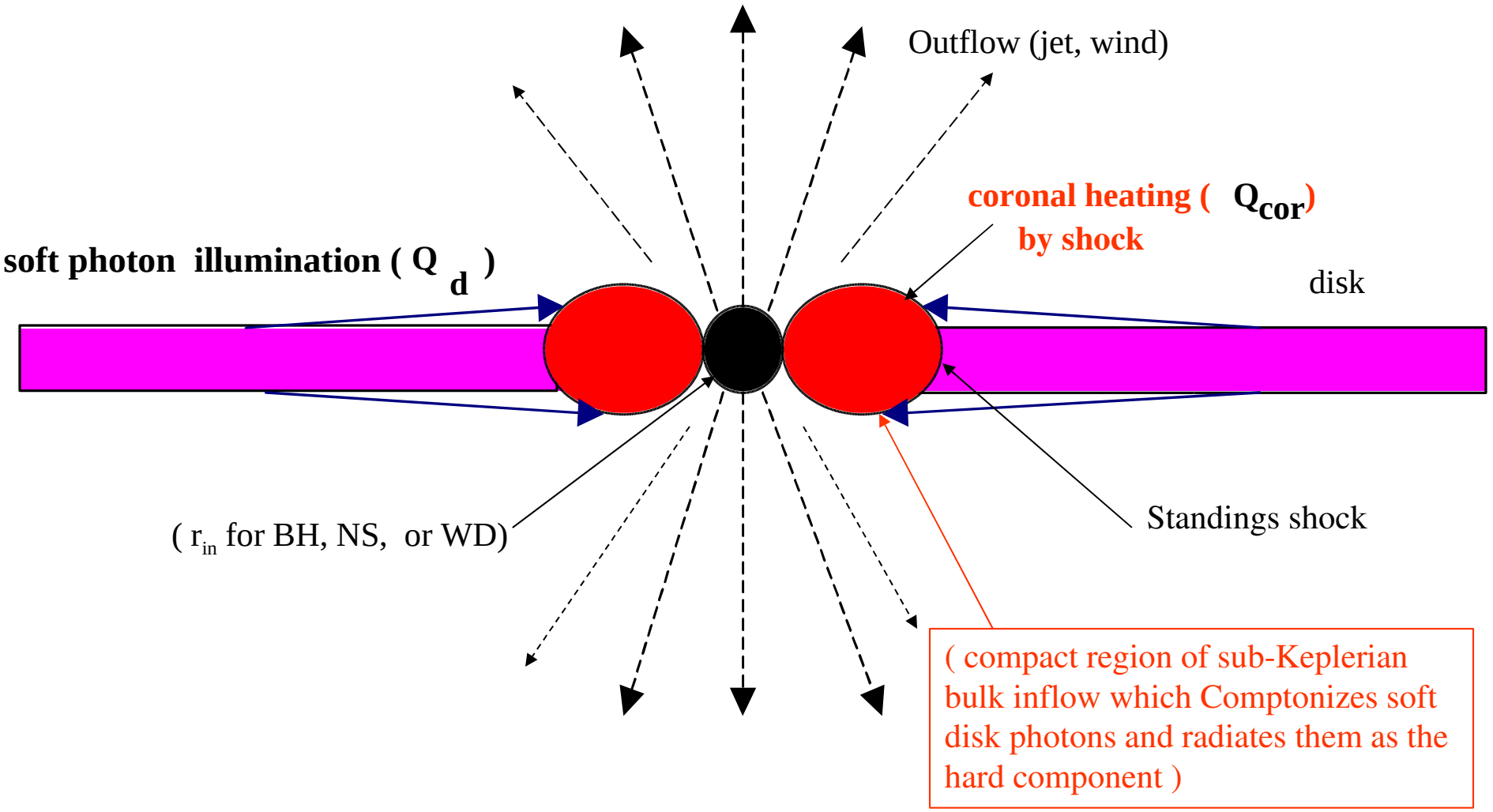

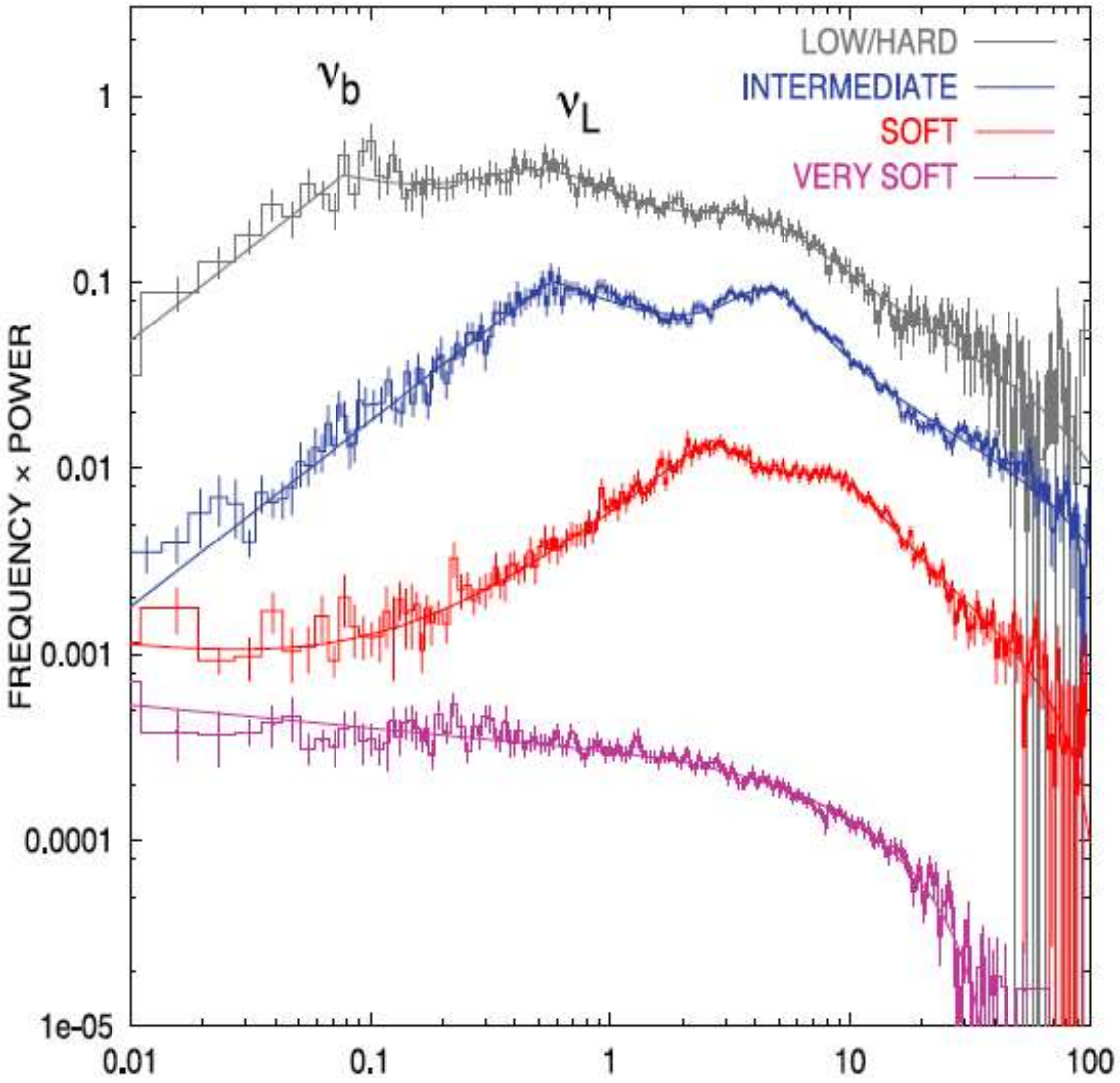

Shaposhnikov & T (2006)

FIG. 6.—Power spectrum (PDS) evolution of the source from the low/hard state (*gray lines*) through the intermediate state (*blue lines*) and soft state (*red lines*) to the very soft state (*purple lines*). The break frequency ν_b and the low QPO frequency are clearly seen in the low/hard, intermediate, and soft states. In the very soft state the power spectrum is featureless; neither QPO nor break are present. Any break and QPO features are washed out.

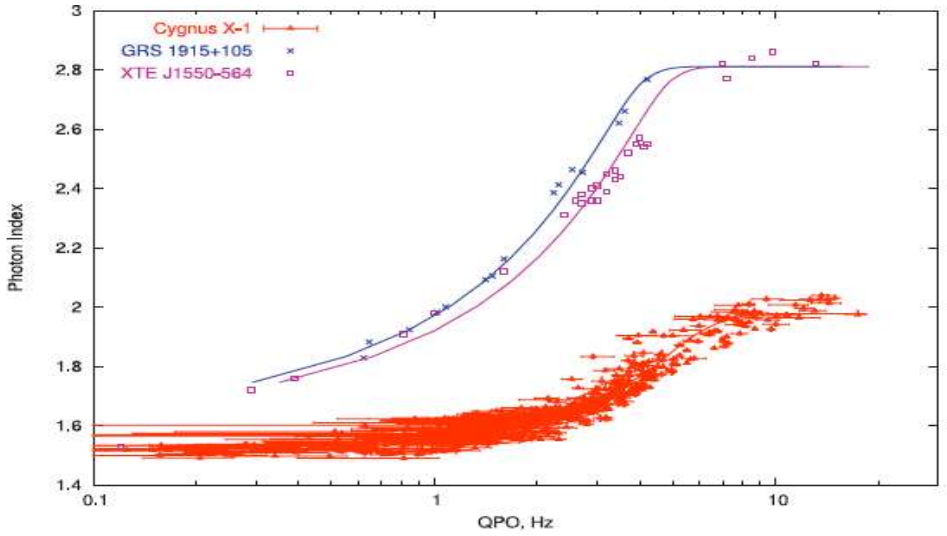

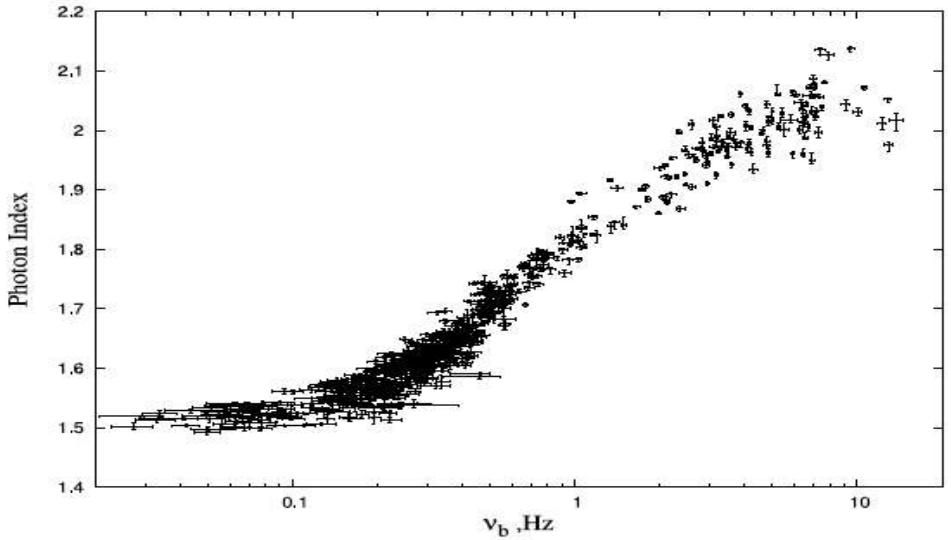

FIG. 8.—*Top*: Observed correlations between photon index Γ and low frequency ν_L (*red points*) compared with those in two other BHC sources, XTE J1550−564 and GRS 1915+105. The saturation value of the index varies from source to source, but it does not exceed the theoretically predicted value of 2.8 for the converging flow of nonrelativistic temperature (see TZ98). Presumably, the saturation value of the index depends on the plasma temperature of the converging flow (LT99). *Bottom*: Observed correlation between photon index Γ and break frequency ν_B for Cyg X-1.

Index- low QPO frequency correlation in BH candidates

Shaposhnikov & T (2006)

Ratio of sub-harmonic frequency to the low frequency

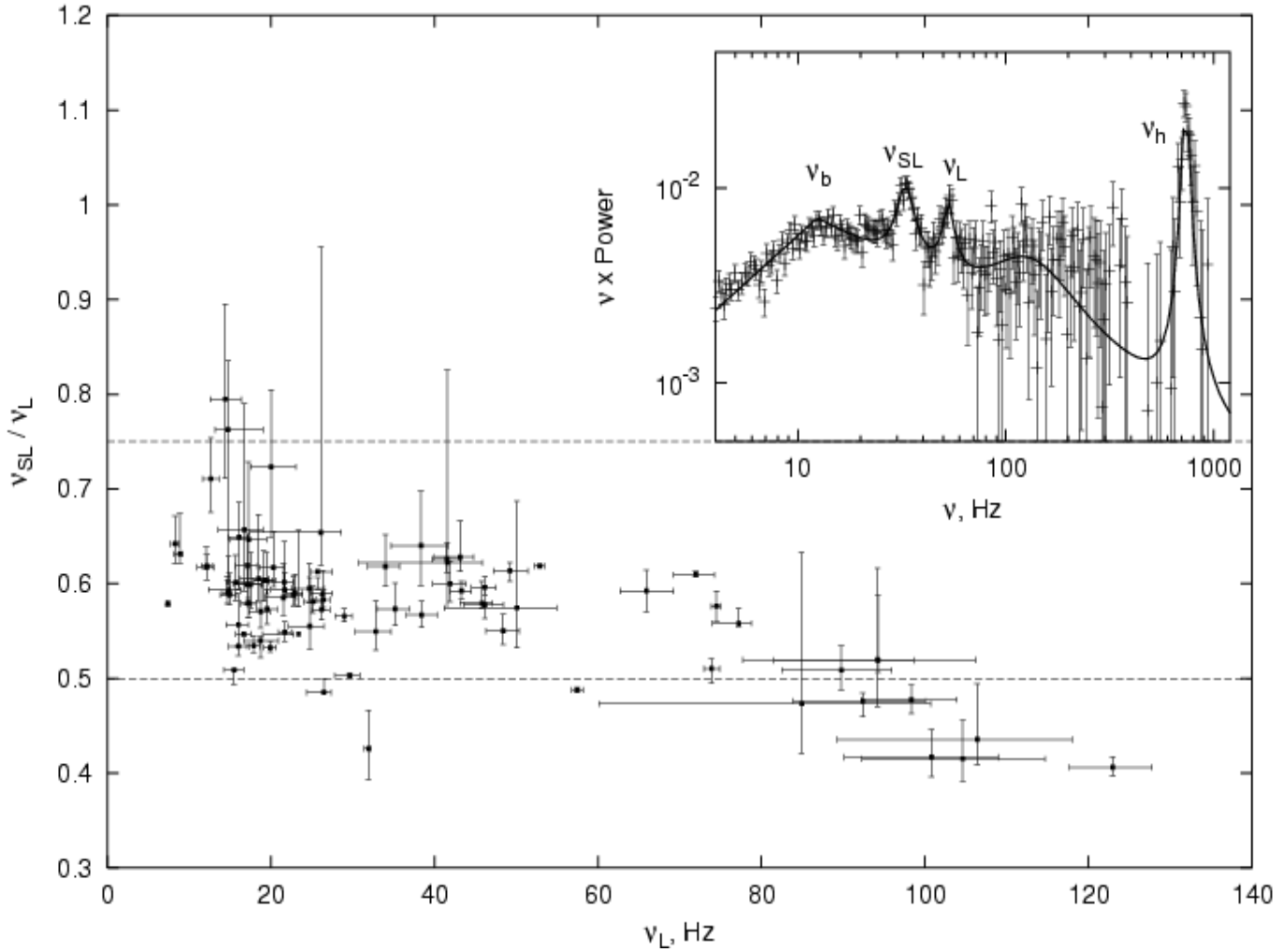

Observed ratio of sub-harmonic frequency of the low frequency ν_{SL} to low frequency ν_L as a function of ν_L . Two horizontal lines indicate the corridor where the most of ratio points are situated.

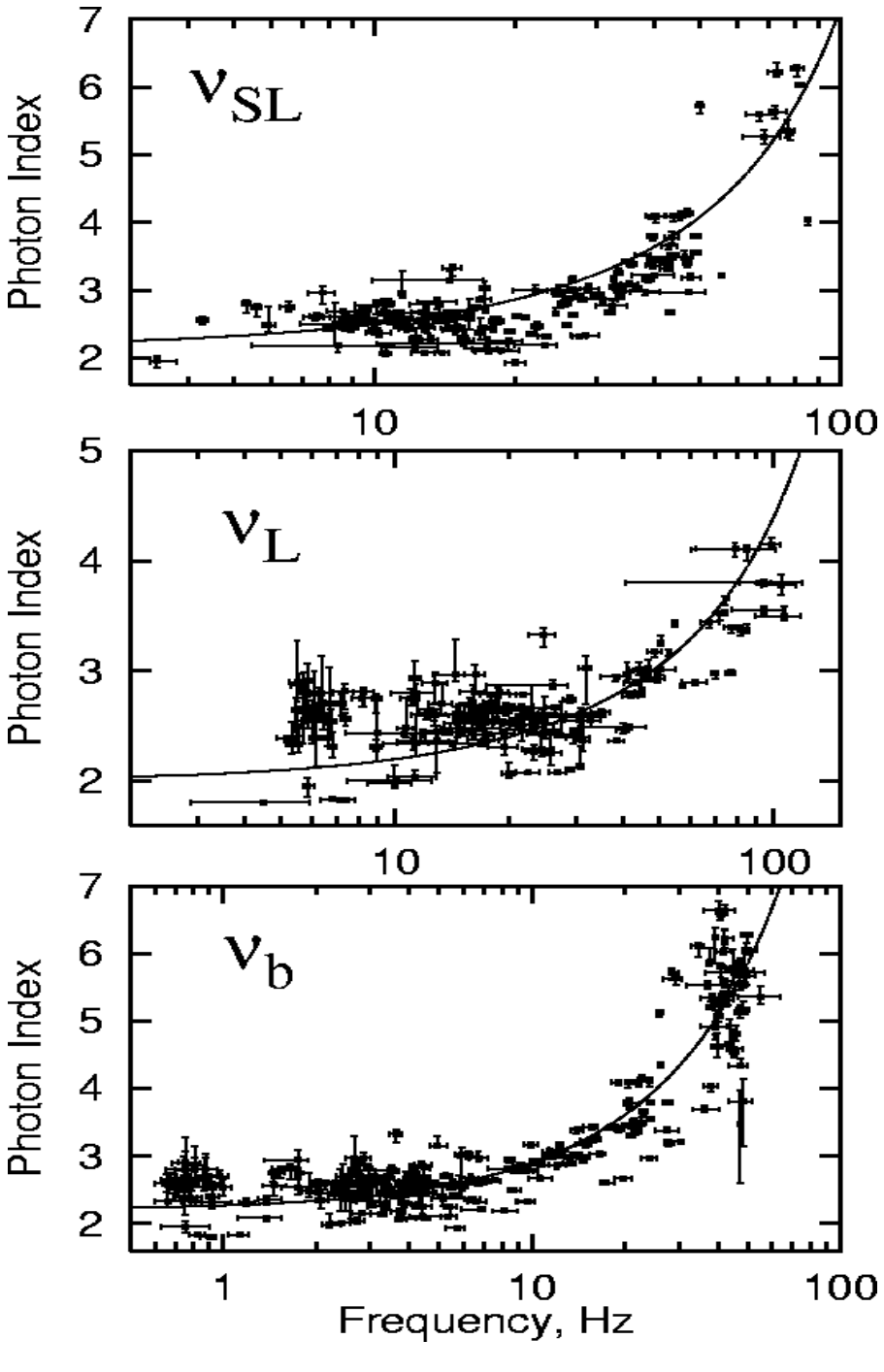

Index-QPO frequency correlation for NS source 4U 1728-34

T & Shaposhnikov (2005)

BH mass determination:Cyg X-1

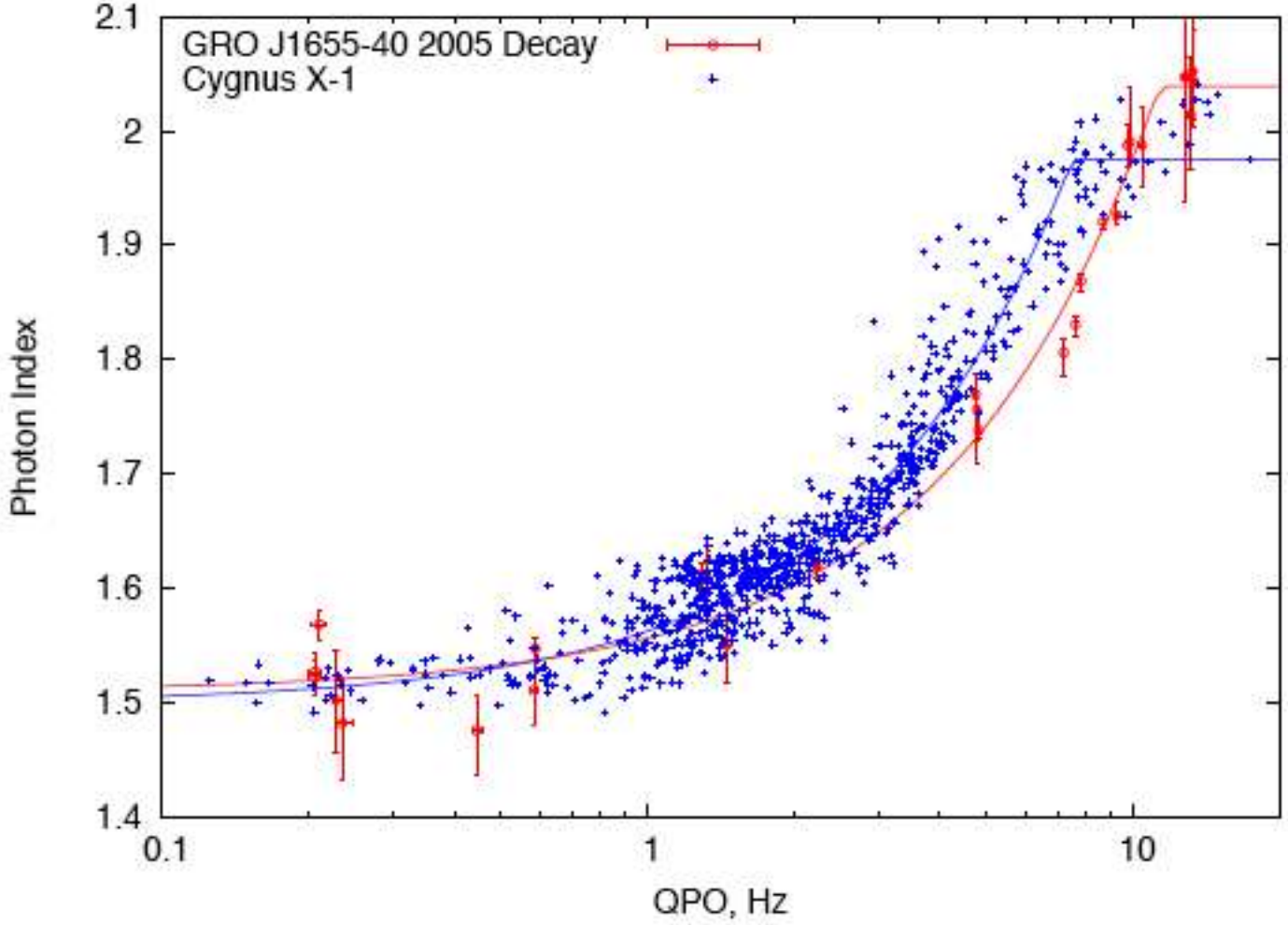

Fig. 2.— Determination of BH mass in Cyg X-1. Correlations for Cyg X-1 comprises RXTE-mission-long data from ST06 (blue color). Data for GRO 1655-40 is for the 2005 outburst decay. The sources show similar saturation levels for both ends of correlation. Index-QPO correlation scaling gives for the BH mass in Cyg X-1 $M_{CygX-1} = 8.5 \pm 1.2\, M_{\odot}$.

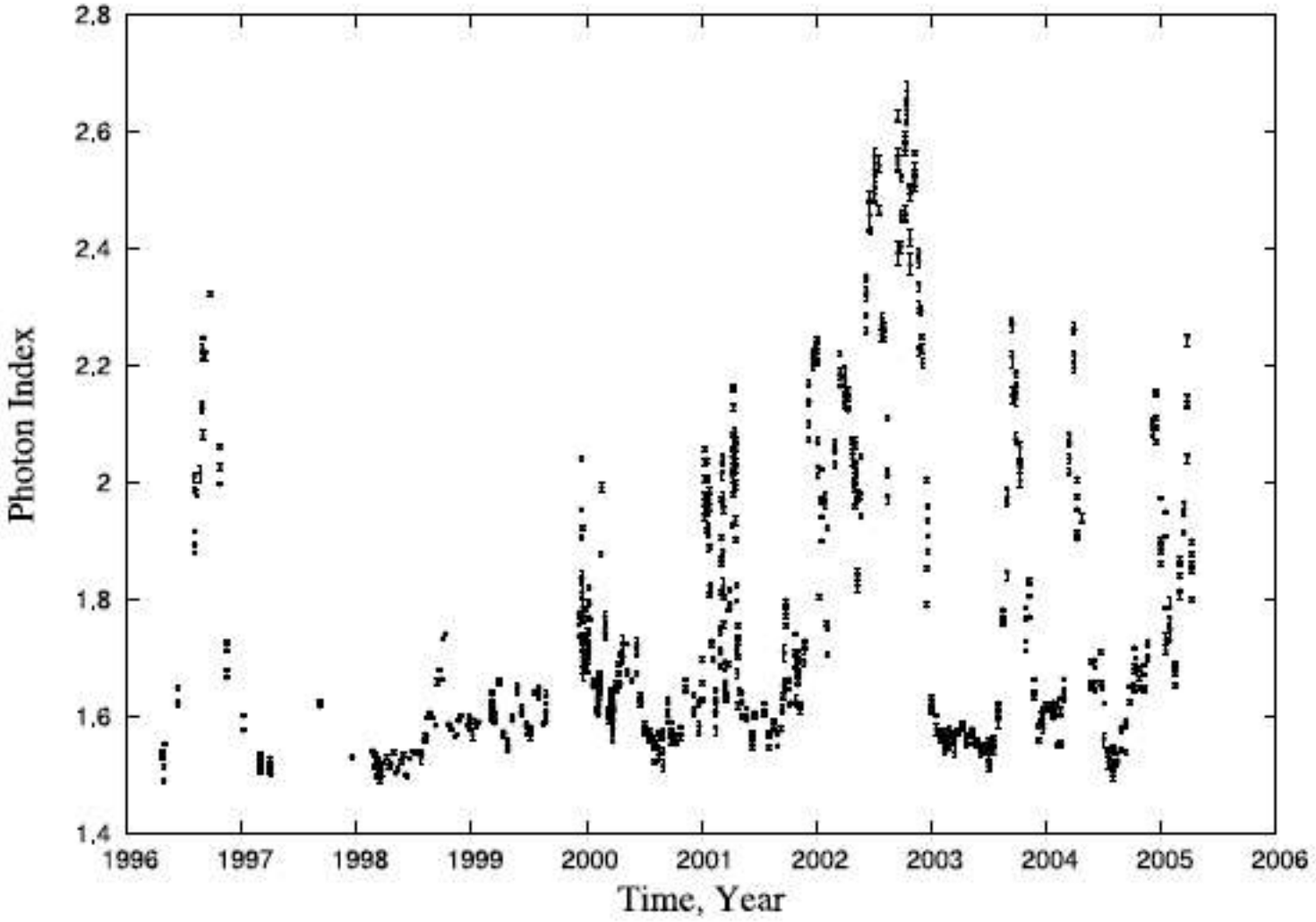

FIG. 15.—The variation of the photon index in Cyg X-1 throughout the entire *RXTE* mission.

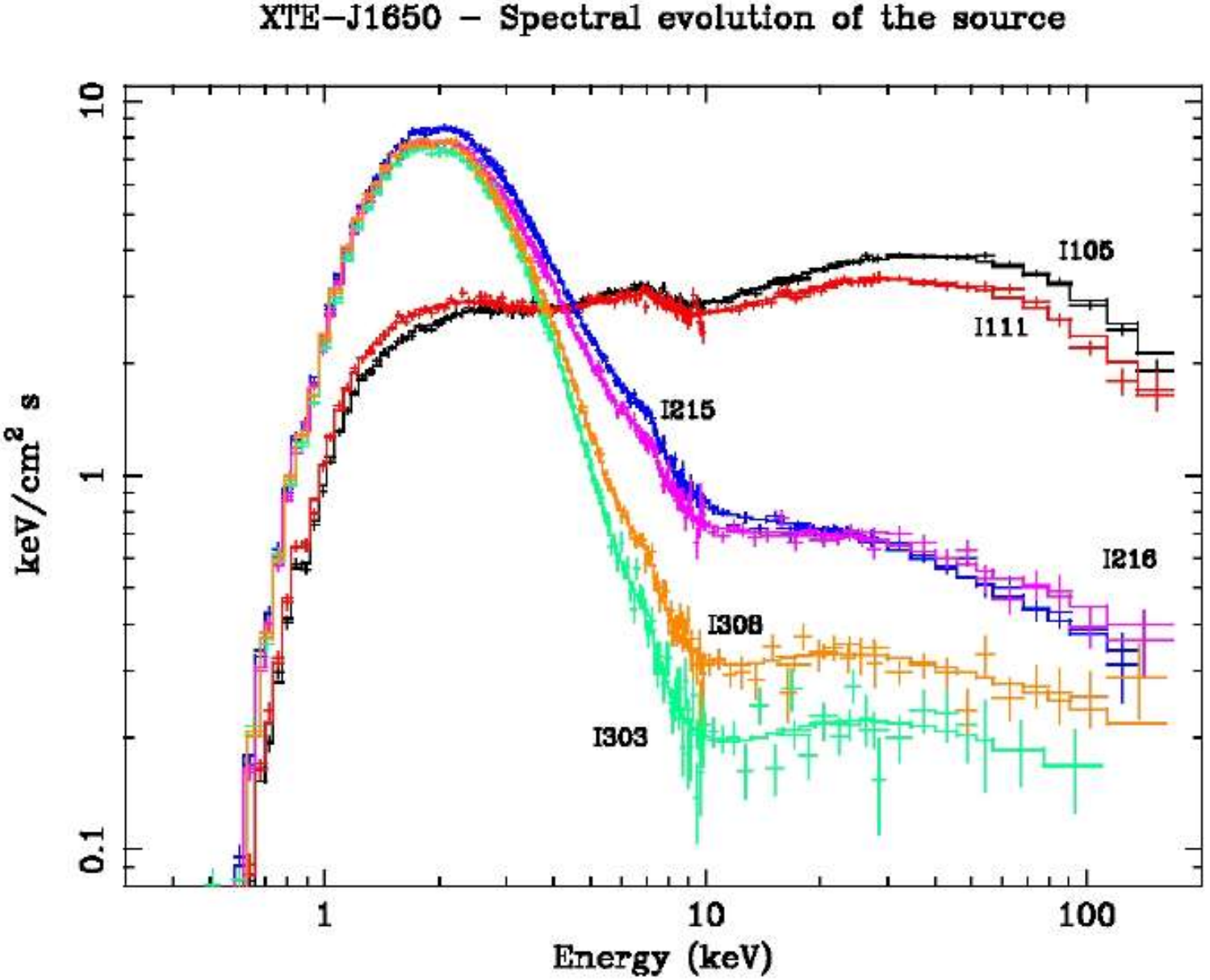

Montanari, T & Frontera 2006

PDS - harder part (blue) and softer part (red) of Hard State of XTE-J1650 (TOO1)

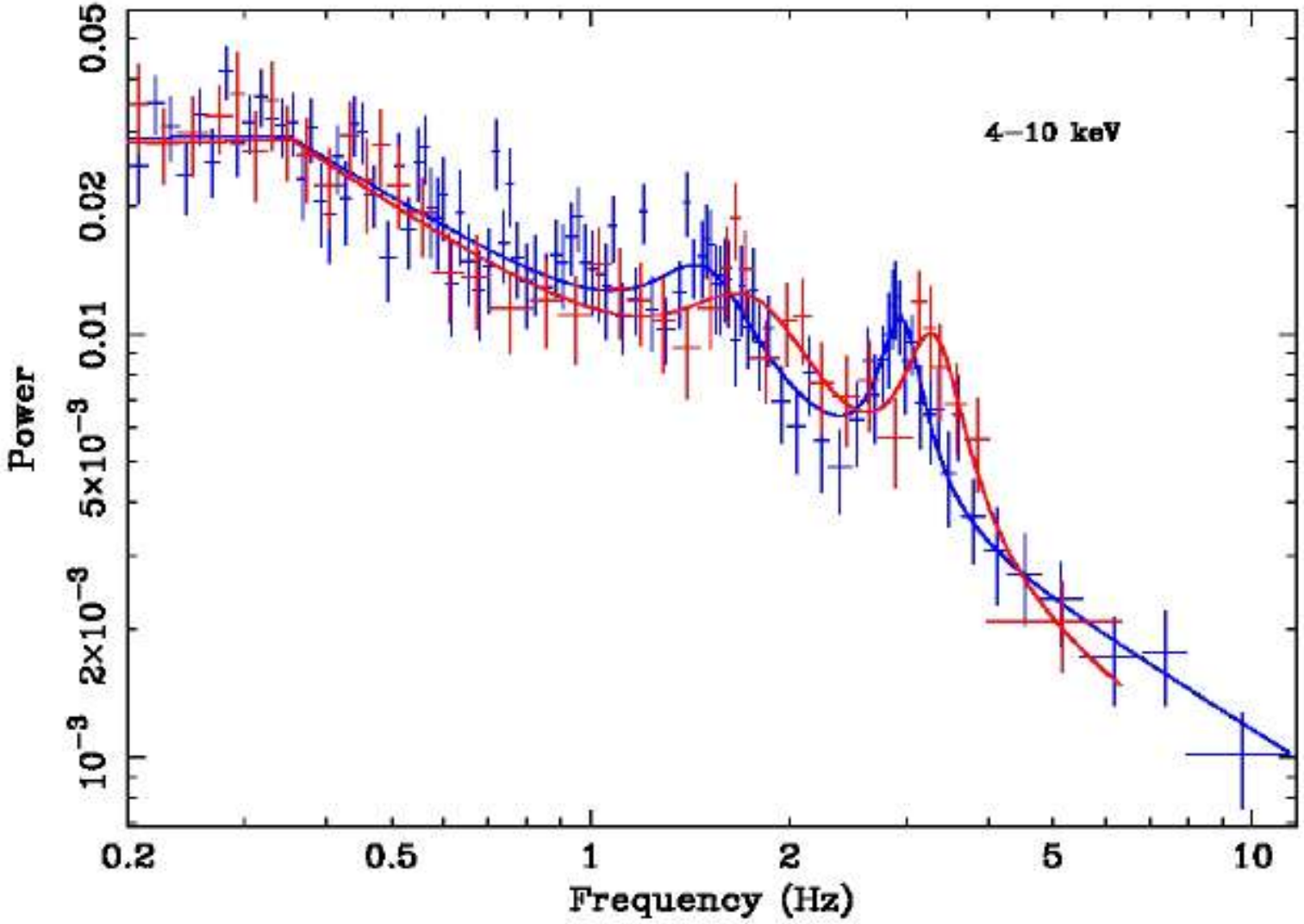

Montanari, T & Frontera 2006

PDS for different energy ranges for TOO1

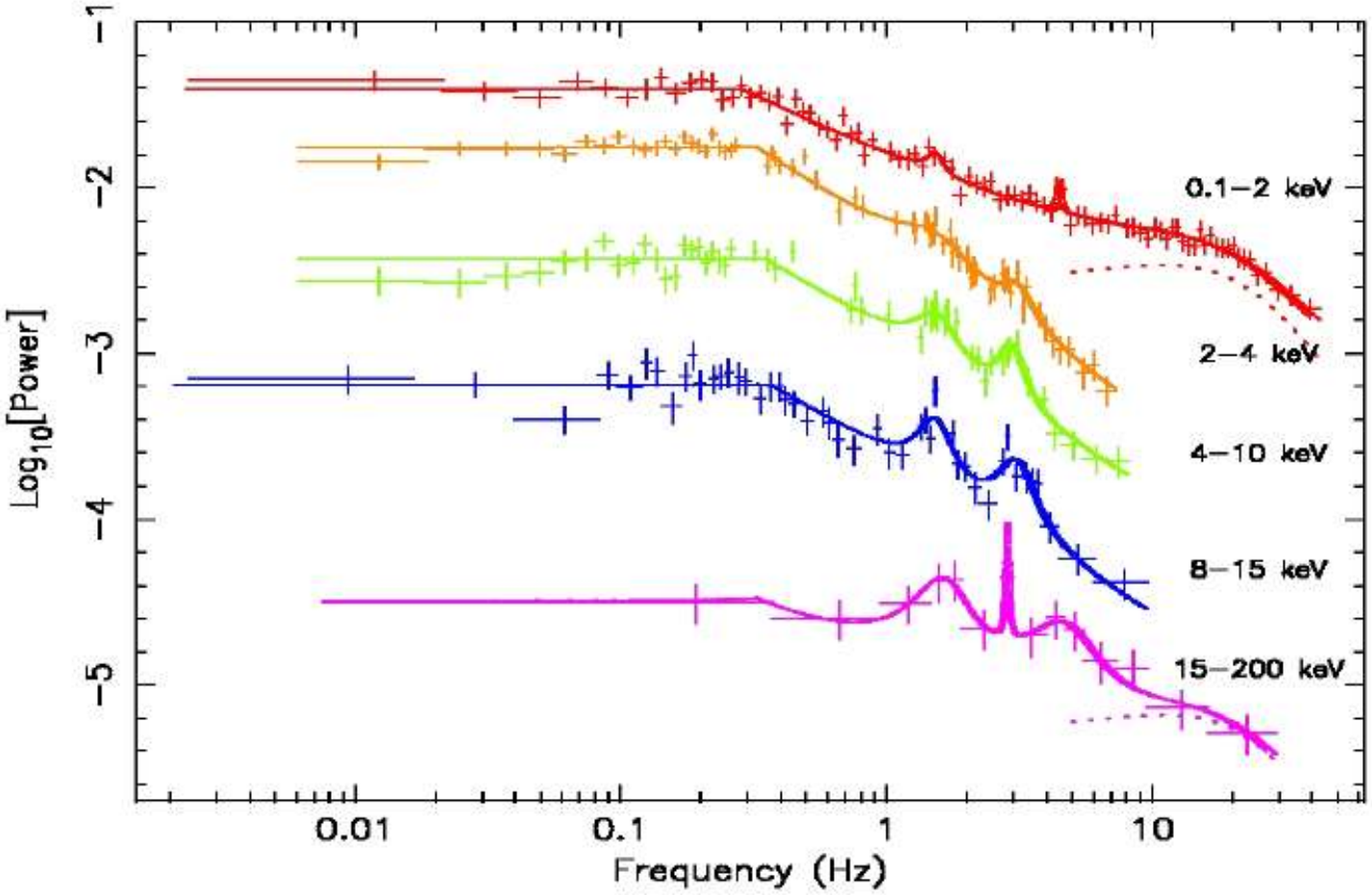

Montanari, T & Frontera 2006

Evolution of the PDS of XTE-J1650 during its spectral change from Hard to Soft state

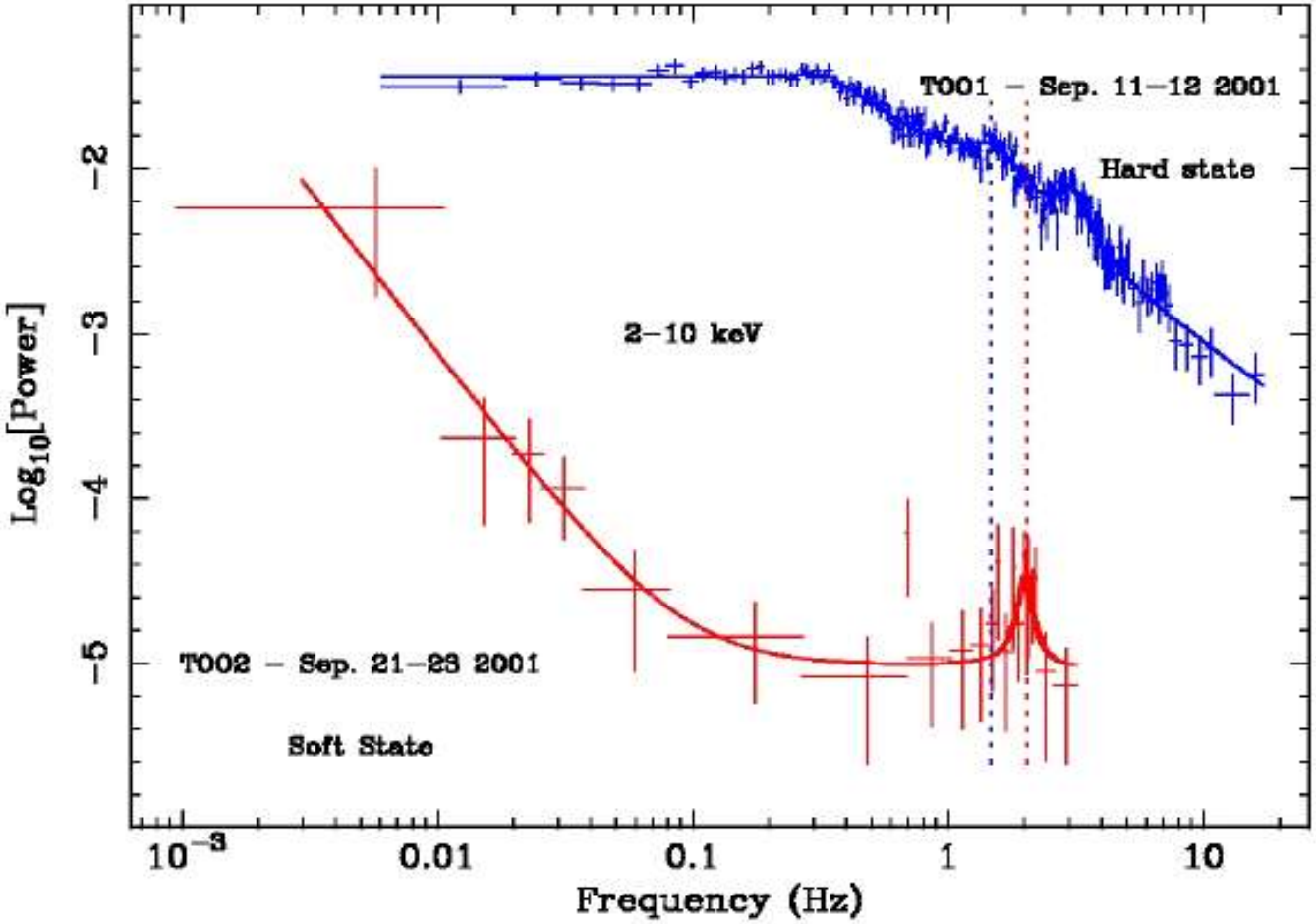

Montanari, T & Frontera 2006

XTE-J1650 (BH)

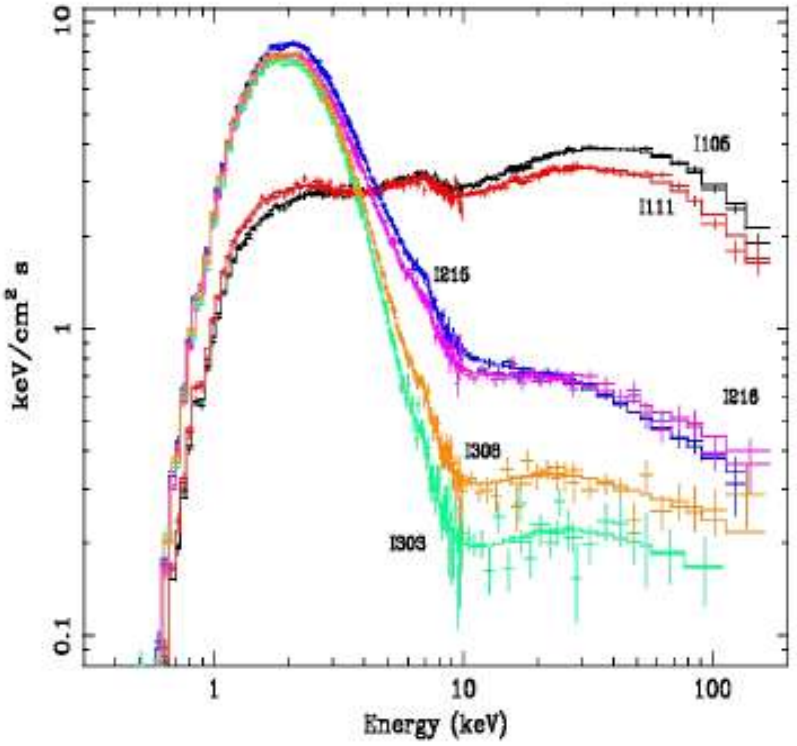

4U 1728-34 (NS)

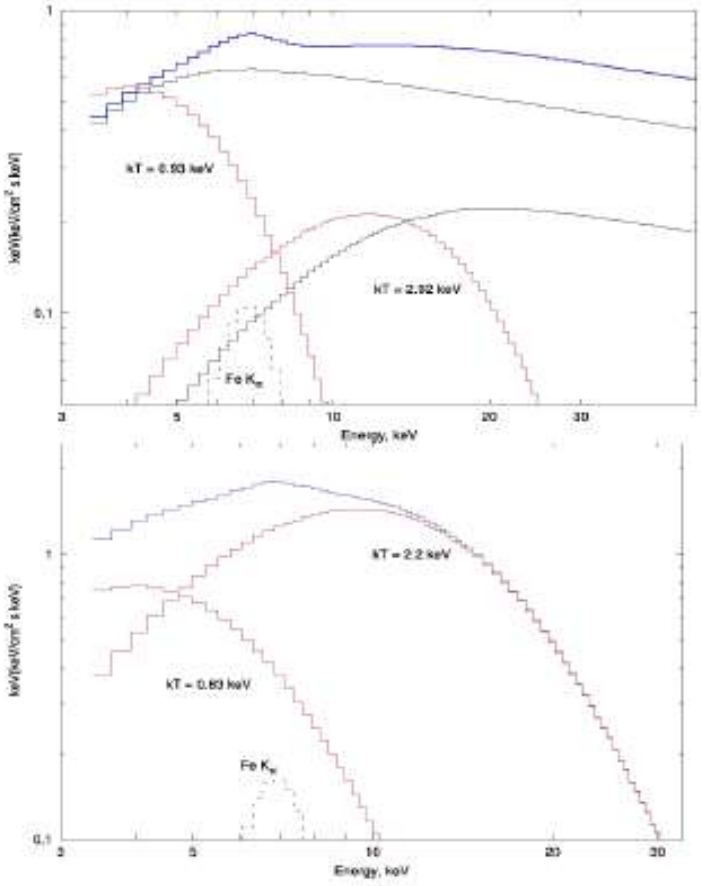

Titarchuk & Shaposhnikov (2005) ApJ 626, 298

Diffusive propagation of the perturbation in the disk

Formulation of the problem

The diffusion equation for the time variable quantity $W(R,t)$, related to the surface density perturbations $\Delta\Sigma(R,t)$, $W(R,t) = \Delta\Sigma(R,t)$, can be written in an operator form

$$\frac{\partial W}{\partial t} = \mathbf{\Lambda_R} W + \varphi(t) f(R) \tag{2}$$

where R is a radial coordinate in the disk and $\mathbf{\Lambda_R}$ is the space diffusion operator. Equation (2) should be combined with the appropriate boundary conditions at $R = 0$, $R = R_0$ and initial conditions at $t = 0$. For homogeneous initial conditions, namely for $W(R,0) = 0$ the solution at any R and t can be presented as a convolution

$$W(R,t) = \int_0^t \varphi(t') X(R, t-t') dt'. \tag{3}$$

The kernel of convolution (3), $X(R,t-t')$ is a solution of the initial value problem for the homogeneous equation

$$\frac{\partial X}{\partial t} = \mathbf{\Lambda_R} X \tag{4}$$

with the following initial conditions

$$X(R,t-t')_{t=t'} = X(R,0) = f(R) \tag{5}$$

The power spectrum $||F_W(\omega)||^2$ of $W(R,t)$ can be presented as a product of the power spectra $||F_\varphi(\omega)||^2$ and $||F_X(\omega)||^2$ of $\varphi(t)$ and $X(R,t)$ respectively:

$$||F_W(\omega,R)||^2 = ||F_\varphi(\omega)||^2||F_X(\omega,R)||^2, \tag{6}$$

The X-ray resulting variable signal is determined by the fluctuations of the luminosity $\Delta L_x(t)$. We assume that the mass accretion rate variations $\Delta\dot{M}(0,t)$ is converted with efficiency ε_{eff} into the variations of the X-ray luminosity, i.e. $\Delta L_x(t) = \varepsilon_{eff}\Delta\dot{M}(0,t)$.

W01 show that for the function $\mathcal{W}(x,t) = x\hat{\nu}W(x^2,t)$ using a new variable $x = R^{1/2}$ the diffusion equation (2) can be presented in the form

$$\frac{\partial\mathcal{W}}{\partial t} = \frac{3\hat{\nu}(x)}{4x^2}\frac{\partial^2\mathcal{W}}{\partial x^2} + \varphi(t)\mathcal{F}(x)$$

where $\hat{\nu}(x)$ is viscosity in the disk, $\mathcal{F}(x) = x\hat{\nu}(x)f(x^2)$. The convolution, similar to Eq. (3), presents the solution $\mathcal{W}(x,t)$

$$\mathcal{W}(x,t) = \int_0^t \varphi(t')\mathcal{X}(x,t-t')dt'$$

where $\mathcal{X}(x,t)$ is a solution of the initial value problem (compare with Eqs. 4, 5)

$$\frac{\partial\mathcal{X}}{\partial t} = \frac{3\hat{\nu}(x)}{4x^2}\frac{\partial^2\mathcal{X}}{\partial x^2}$$

with the following initial conditions

$$\mathcal{X}(x,0) = \mathcal{F}(x).$$

The boundary condition at the outer boundary $\dfrac{\partial \mathcal{X}}{\partial x} = 0 \quad \text{at} \quad x = x_0$

Assumed that at the inner boundary $x_{\rm in} \ll x_0,\ W = \Delta\Sigma = 0,$ *which is equivalent to*

$$\mathcal{X} = 0 \quad \text{at} \quad x = x_{\rm in}.$$

We assume that perturbations of the mass accretion rate at the inner disk edge is converted with efficiency $\varepsilon_{\rm eff}$ *into perturbations of the X-ray luminosity, i.e.*

$$\Delta L(t) = \varepsilon_{\rm eff} \Delta \dot{M}(t, R_{in})$$

Because $\Delta \dot{M} = 3\pi \dfrac{\partial \mathcal{X}}{\partial x}$ *then* $Y(t) \propto \Delta L_x(t) \propto \dfrac{\partial \mathcal{X}}{\partial x}(t, 0).$

Now we consider a general case of problems where $\hat{\nu}(x) = (\hat{\nu}_0 / x_0^{\psi}) x^{\psi}.$

a. Viscosity linearly distributed over radius: $\psi = 2$

$$Y(t) \propto \sum_{k=1}^{\infty} \exp[-\pi^2 (2k-1)^2 t / 4t_0].$$

where the viscous time scale $t_0 = 4x_0^4 / 3\hat{\nu}_0 = 4R_0^2 / 3\hat{\nu}(R_0).$

Then the power spectrum of Y(t) is: $||F_Y(\nu)||_\nu^2 \propto \sum_{k=0}^{\infty} \dfrac{1}{(8t_0\nu/\pi)^2 + (2k+1)^4}.$

The series in the right hand side of this equation can be calculated exactly

$$||F_Y(\nu)||^2_\nu \propto \frac{\pi}{2^{3/2}a^{3/2}} \frac{\sinh 2^{1/2}\pi a^{1/2} + \sin 2^{1/2}\pi a^{1/2}}{\cosh 2^{1/2}\pi a^{1/2} - \cos 2^{1/2}\pi a^{1/2}} -$$

$$- \frac{\pi}{2^{5/2}a^{3/2}} \frac{\sinh \pi a^{1/2}/2^{1/2} + \sin \pi a^{1/2}/2^{1/2}}{\cosh \pi a^{1/2}/2^{1/2} - \cos \pi a^{1/2}/2^{1/2}}$$

where $a = 8t_0\nu/\pi.$

As it follows from this formula that

$$||F_Y(\nu)||^2_\nu = C_N \times \pi^4/96 \qquad \text{when} \quad \nu \ll \pi/8t_0$$

and $$||F_Y(\nu)||^2_\nu = C_N \times \frac{1}{2^7\pi^{1/2}t_0^{3/2}} \frac{1}{\nu^{3/2}} \qquad \text{when} \quad \nu \gg \pi/8t_0.$$

General case

Although the series of power spectrum

$$||F_Y(\nu)||^2_\nu \propto \sum_{k=1}^{\infty} \frac{[2k-(10-3\psi)/2(4-\psi)-\varepsilon_k/\pi]^\delta}{(8t_0\nu/\pi)^2+[2k-(10-3\psi)/2(4-\psi)-\varepsilon_k/\pi]^4}$$

has to be calculated numerically the asymptotic form of PDS can be easily evaluated analytically:

$$||F_Y(\nu)||^2_\nu = C_N \times \mathcal{A}_L \qquad \text{when} \quad \nu \ll \pi/8t_0$$

$$||F_Y(\nu)||^2_\nu = C_N \times \frac{\mathcal{A}_H}{\nu^{(3-\delta)/2}} \qquad \text{when} \quad \nu \gg \pi/8t_0$$

where

$$\alpha = (3-\delta)/2 = (7-2\psi)/(4-\psi).$$

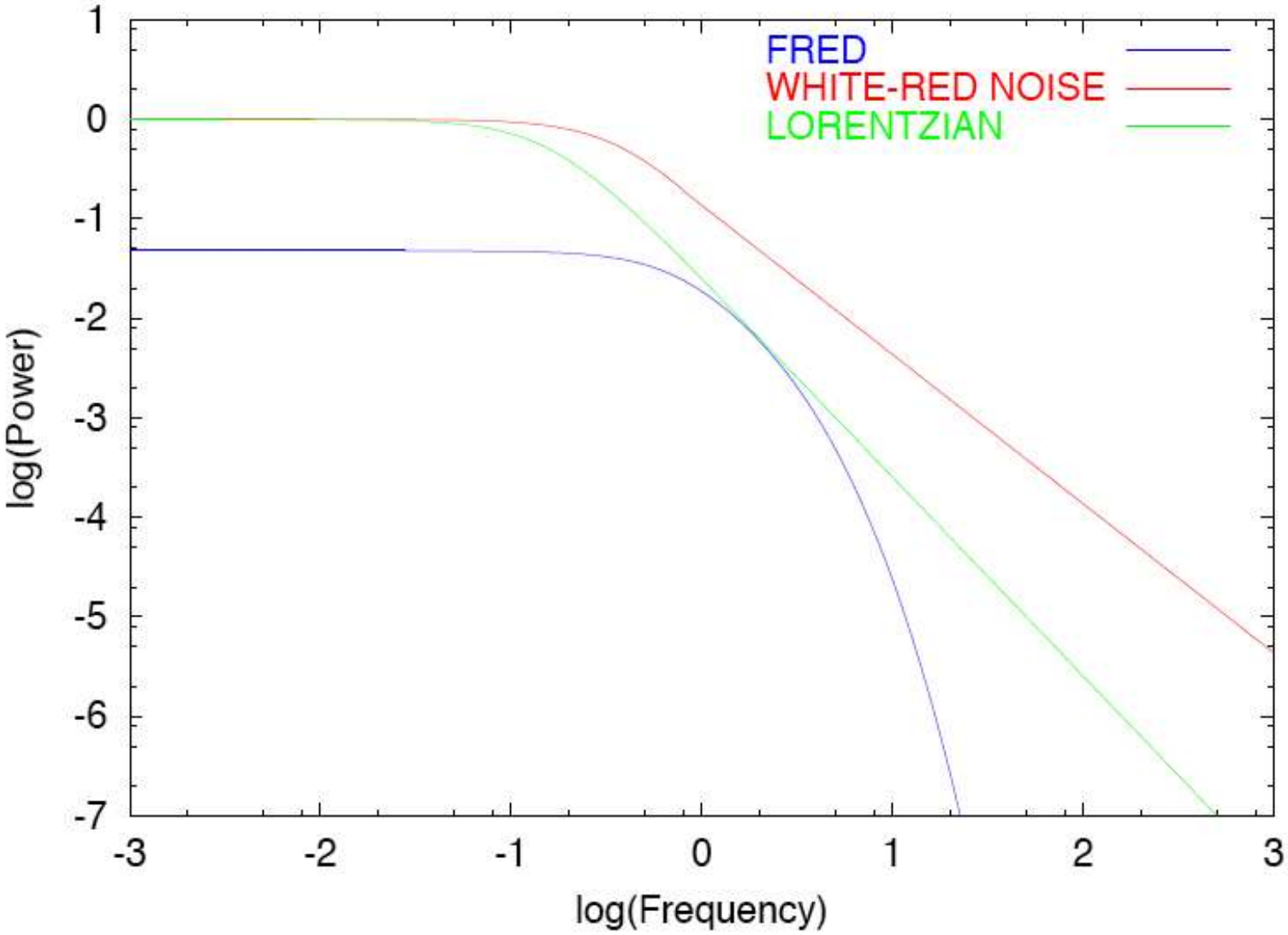

Fig. 1.— Examples of PDS models: PDS of fast rise and exponential decay (FRED) (blue line), PDS of white-red noise (red line) and Lorentzian PDS (green line).

Integrated Power of X-ray emission vs total integrated power of the disk configuration

We obtain that the integrated total power of X-ray resulting signal

$$P_x = \int_0^\infty ||F_x(\omega)||^2 d\omega \sim \frac{1}{D\mathcal{Q}} \frac{P_{dr}}{\omega_{dr} t_0}.$$

We arrive to the conclusion that the resulting integrated power P_x, which is related to the perturbation amplitude at the inner disk edge, is much less than the total integrated power of the driving oscillation in the disk P_{dr}

$$\frac{P_x}{P_{dr}} \sim (D\mathcal{Q}\omega_{dr} t_0)^{-1} \ll 1.$$

Evolution of Power density spectrum and energy spectrum

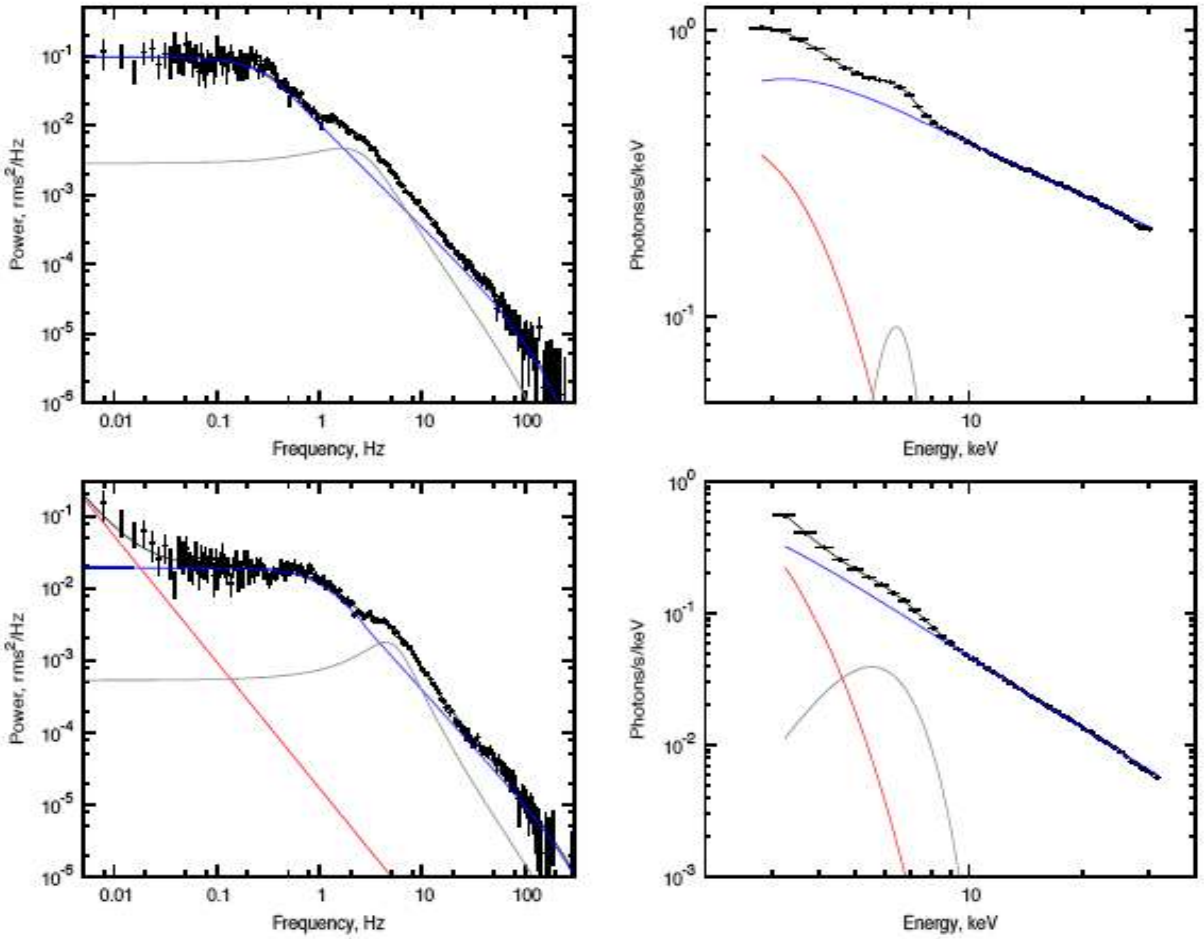

Cyg X-1: Observable power spectrum (PDS) (left panel) vs photon spectrum (right panel). The first observation is a pure low/hard state with no LF WRN component in the PDS. During the second observation the source energy spectrum is still hard, but LF WRN is already detectable.

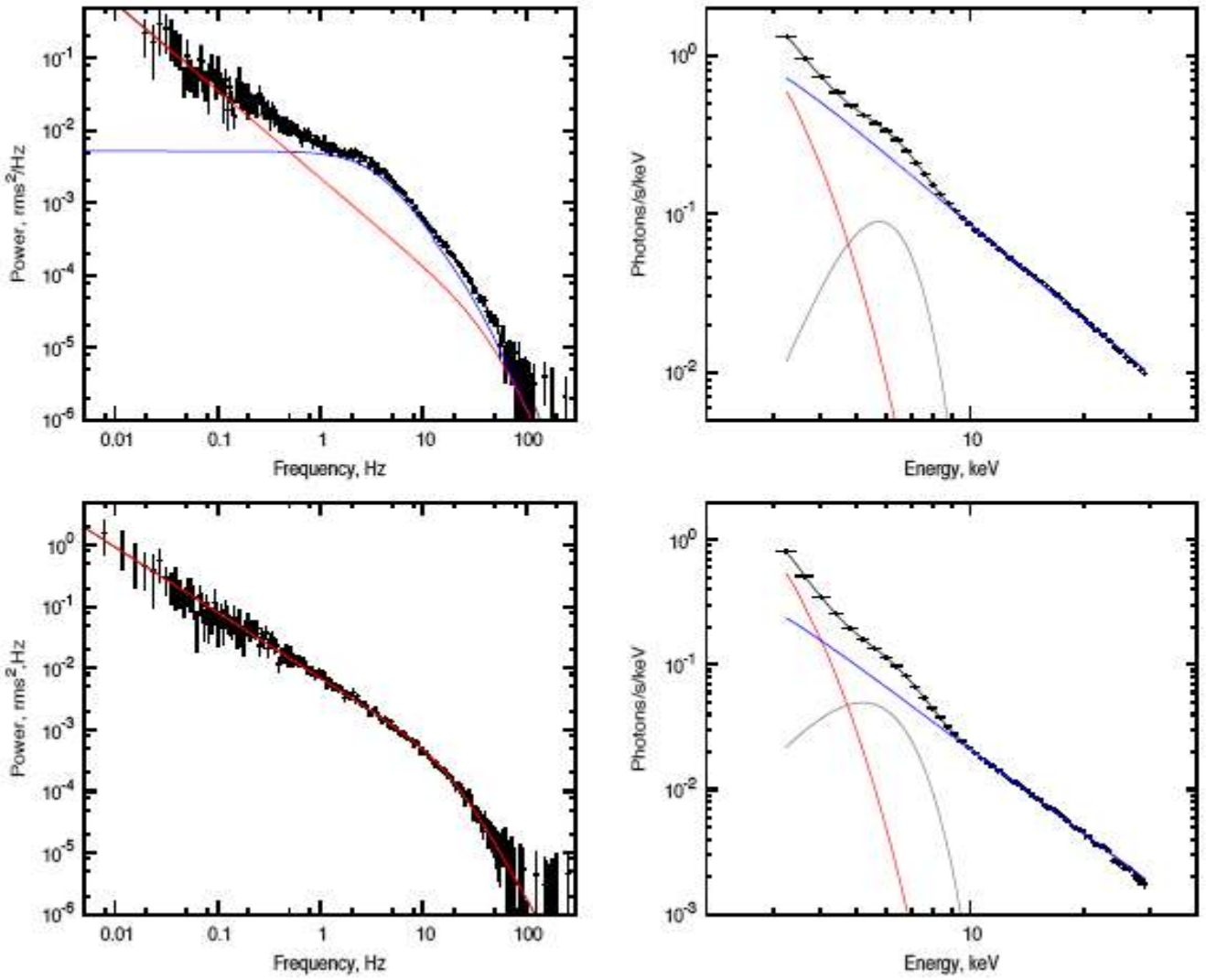

The first observation is taken during the intermediate state just before the transition to high/soft state, which is presented by the second observation.No HF WRN is present in PDS during high/soft state.

Power spectra of Cyg X-1: Hard and intermediate states

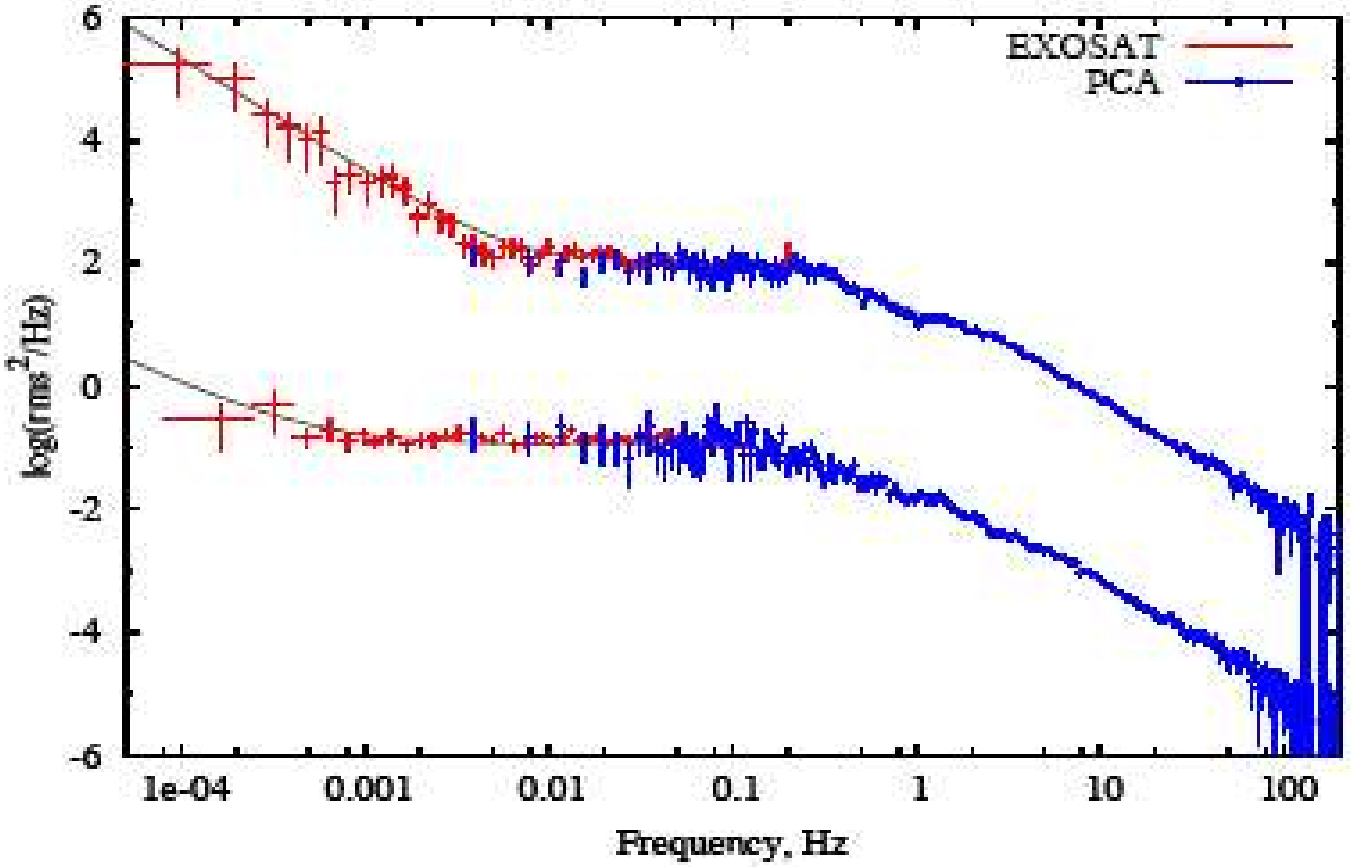

Two composite PDSs: EXOSAT spectra with matching high frequency PCA PDS. Data are fitted by LF-HF diffusion model:

$\chi_2/N_{dof} = 250.1/267 = 0.94$, $\psi_{corona} = 2.32 \pm 0.12$, $t_{0,C} = 1.8 \pm 0.3$, $\psi_D = 2.5$ and

$\chi_2/N_{dof} = 278.5/267 = 1.04$, $\psi_{corona} = 2.07 \pm 0.7$, $t_{0,C} = 1.24 \pm 0.12$, $\psi_D = 0.3 \pm 0.3$.

Soft state power spectrum of Cyg X-1

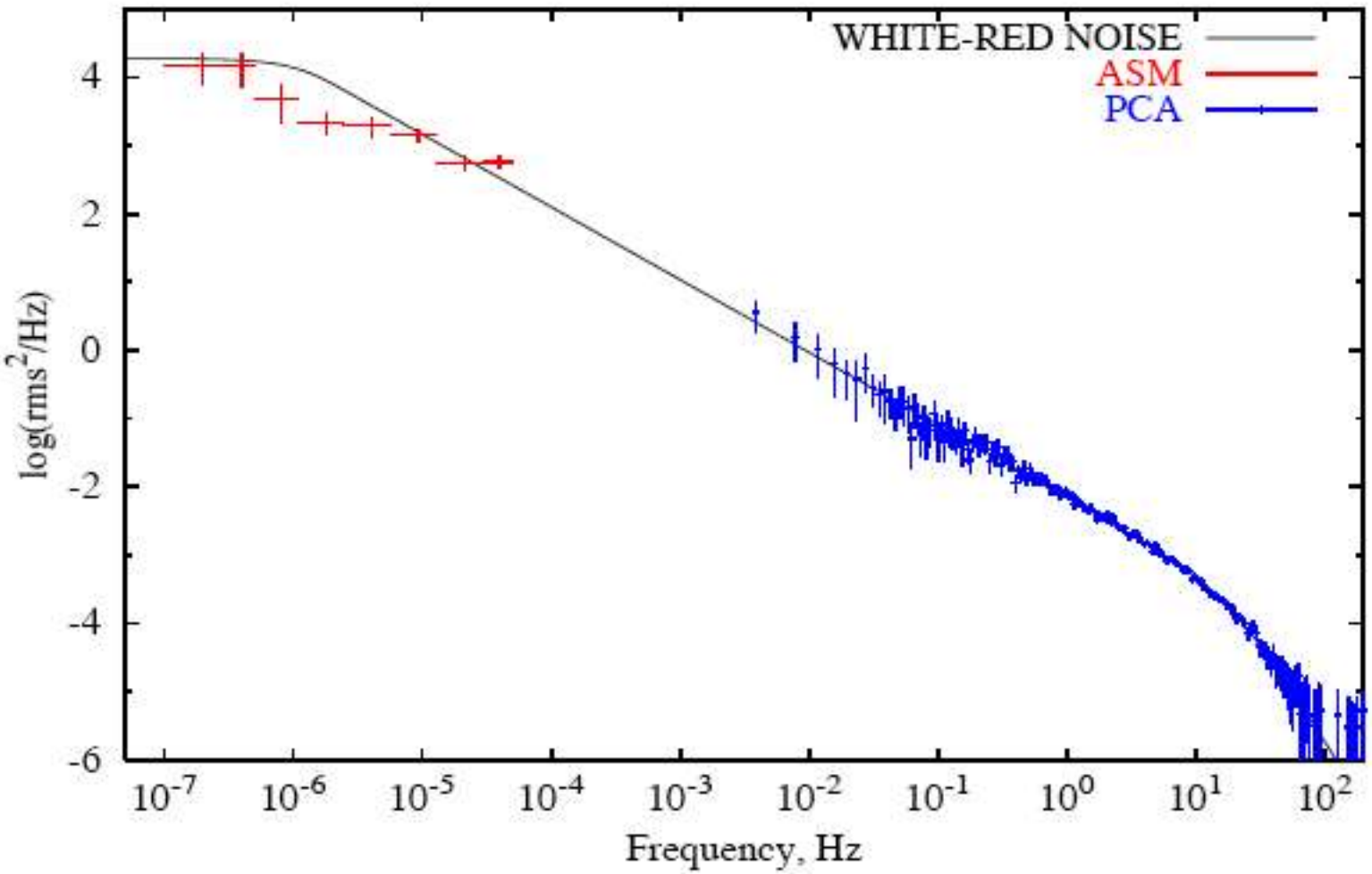

The composite soft state PDS is made by PCA (blue) and ASM (red) PDSs.
The PCA PDS is for ObsID 50110-01-52-00. Data are fitted by LF-HF diffusion model:
$\chi_2/N_{dof} = 184/228 = 0.81$, the best -fit parameters $t_{0,D} = (6 \pm 1.7) \times 10^5$ s, $\psi_D = 2.93 \pm 0.01$.

Composite spectrum of Cyg X-2

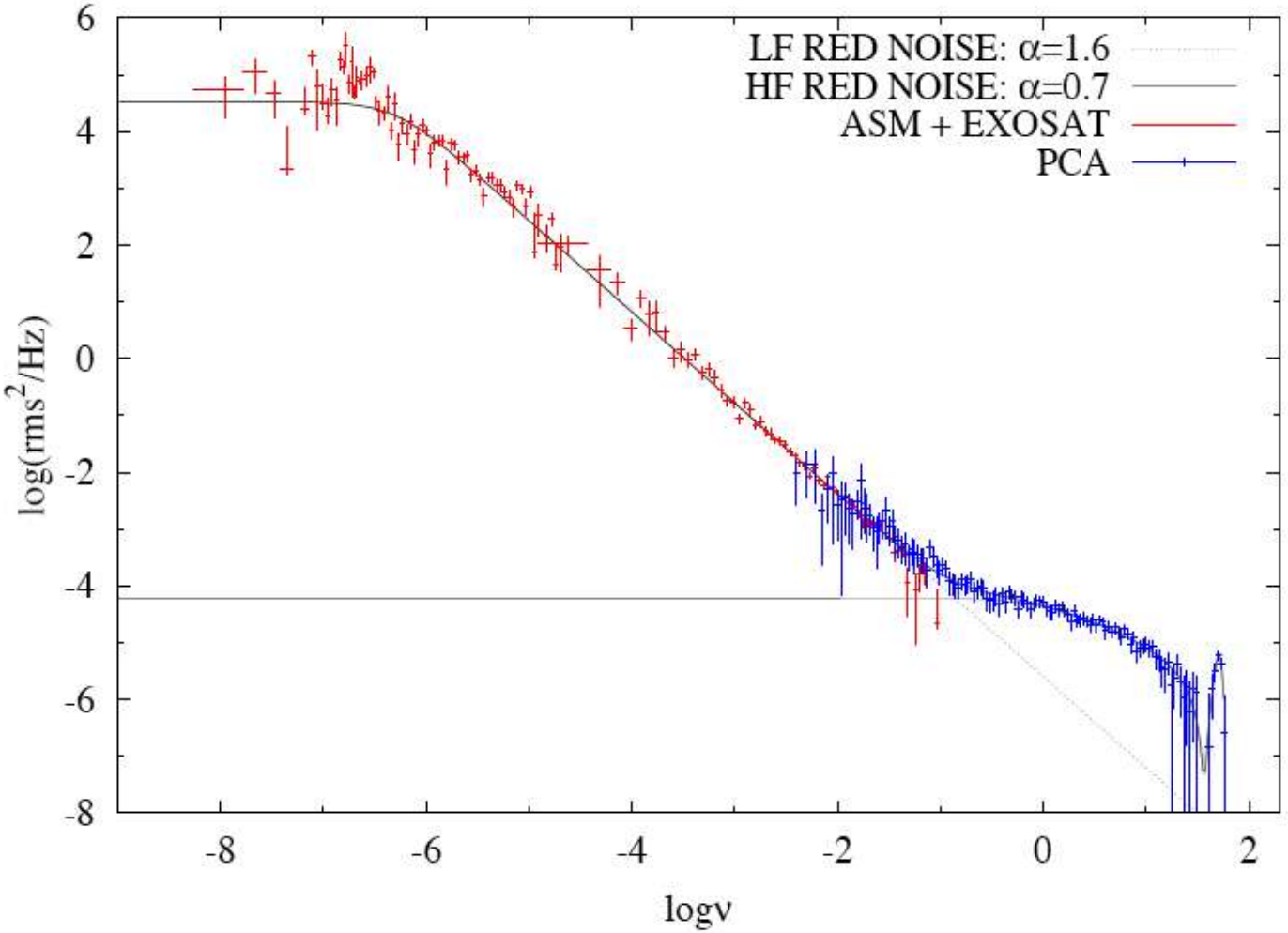

EXOSAT-ASM-PCA (RXTE) power spectrum of Cyg X-2 in frequency range that covers 10 orders of magnitude. One can clearly see low and high frequency (LF and HF) white-red noise components in PDS, related to the extended Keplerian disk and relatively compact, innner disk-like configuration (sub-Keplerian Compton corona) respectively. Each of these two components is perfectly fitted by our white-red noise model (dotted and solid lines are for LF and HF best-fit models respectively.

Reynolds number of the flow and Shakura-Sunyaev disk - alpha parameter as observable quantities

Using the best-fit parameters of the PDS model we can infer the evolution of the physical parameters of the source such the disk diffusion time t_0, magnetoacoustic QPO frequency and Reynolds number of the accretion flow Re, with the change of photon index. We can relate t_0 with Re and magnetoacoustic QPO frequency 

$$t_0 = \frac{4}{3}\frac{4}{(4-\psi)^2}\left[\frac{V_{MA}R_0}{\hat{\nu}(R_0)}\right]\left(\frac{R_0}{V_{MA}}\right) = \frac{4}{3}\frac{4}{(4-\psi)^2}\frac{\mathrm{Re}}{a_{MA}\nu_{MA}},$$

because

$$\nu_{MA} = V_{MA}/(a_{MA}R_0)$$

These formulas leads to equation

$$\mathrm{Re} = a_{AM}\frac{3}{4}\frac{(4-\psi)^2}{4}(\nu_L t_0)$$

that allows us to infer a value of Re using the best-fit model parameters t_0 and the QPO low frequency  ***preferably equals to***  ***.***

Determination of Reynolds number of accretion flow from observations

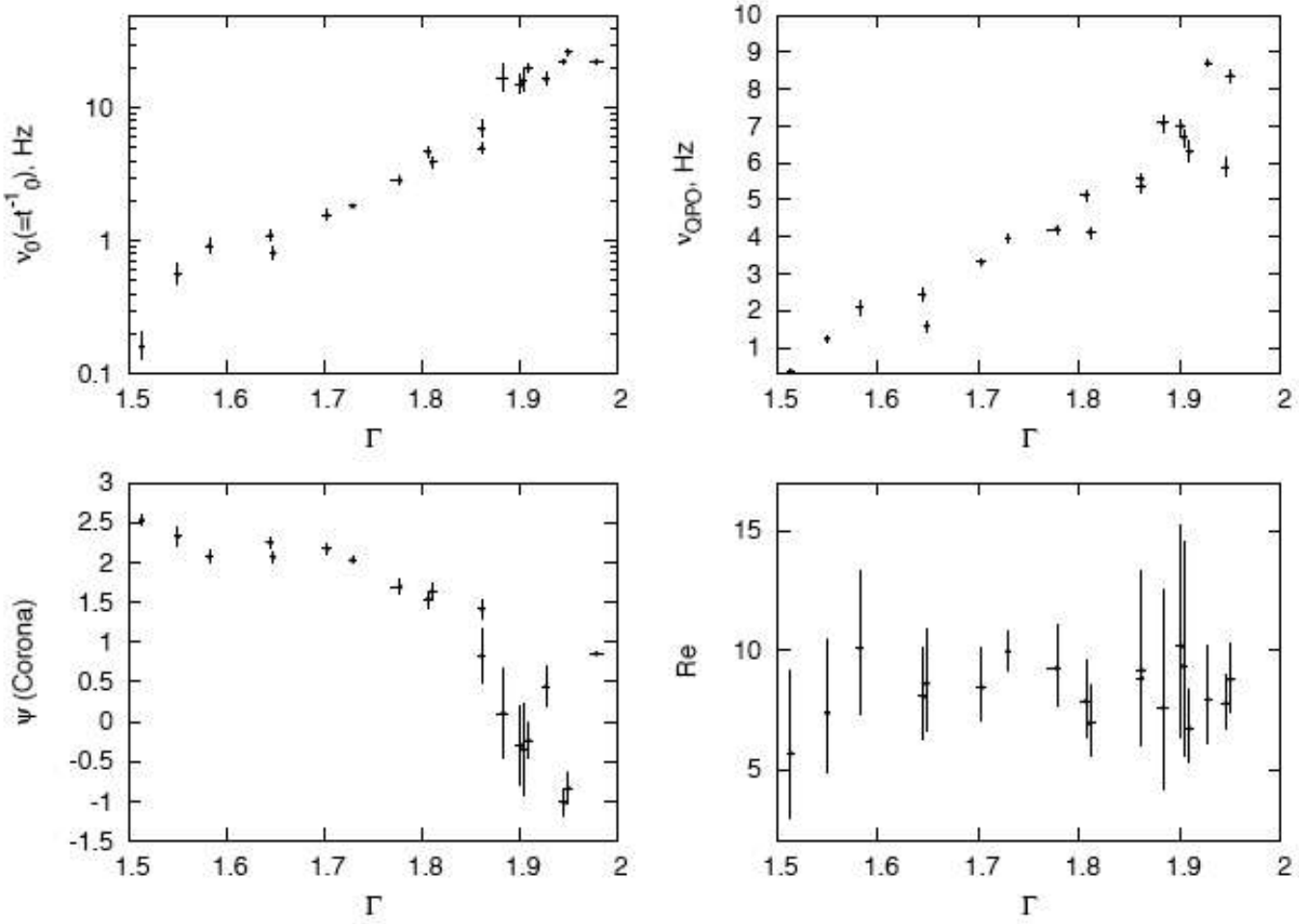

Cyg X-1: HF white-red noise component: the best-fit diffusion frequency $\nu_0 = t^{-1}_0$ vs Γ (upper left panel), QPO low frequency ν_{QPO} (ν_L) vs Γ (right upper panel), the best-fitt index of the viscosity distribution ψ vs Γ (lower left panel) and inferred Reynolds number Re vs Γ (lower right panel).

Observational Evidence of Compton Cloud Contraction

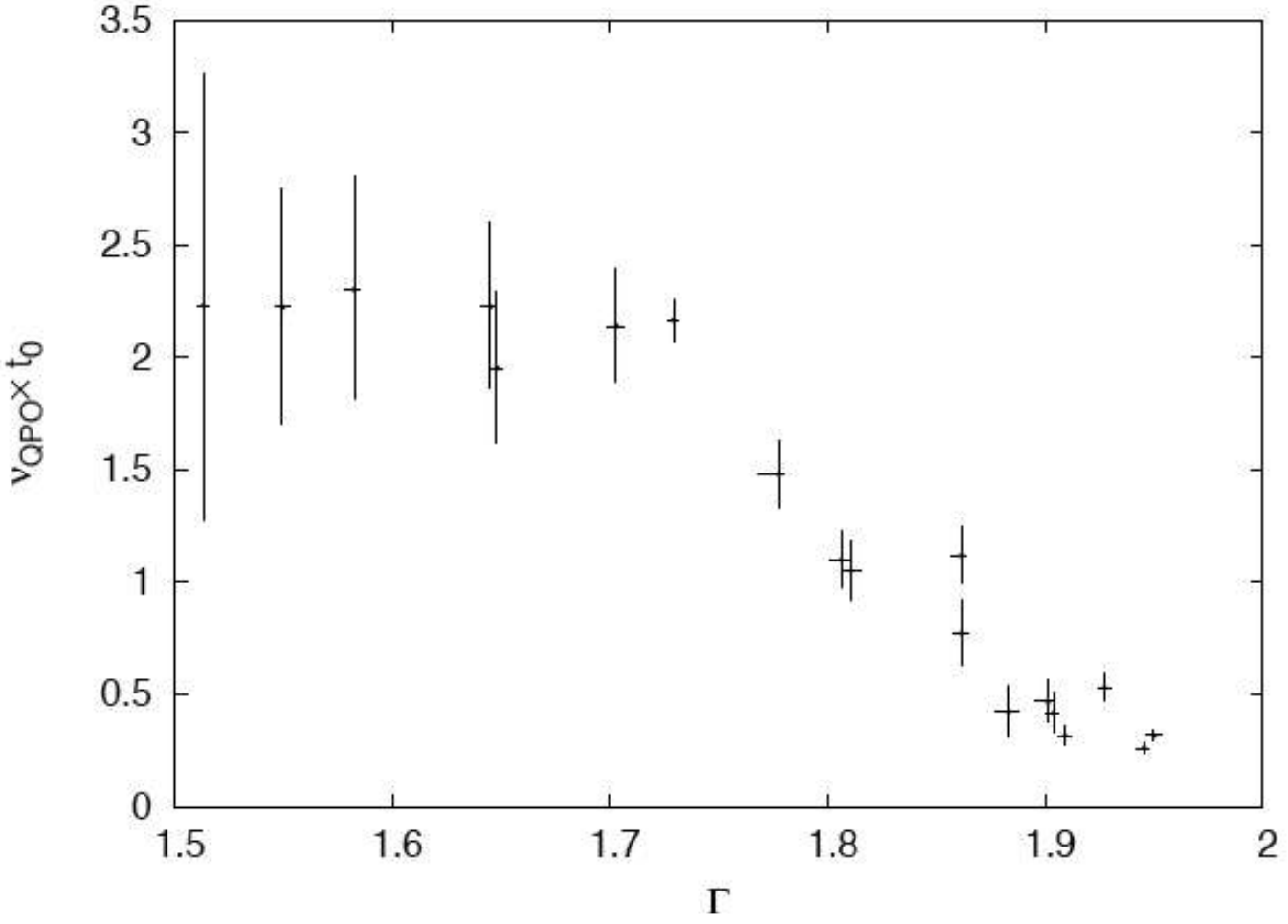

Cyg X-1: a product of QPO low frequency $\nu_{QPO}(\nu_L)$ and the best-fit diffusion time of HF WRN t_0 vs Γ. Decrease of $\nu_{QPO} \times t_0$ with Γ implies that Compton cloud contracts when the source evolves to the softer states.

Driving QPOs in the observed power spectra

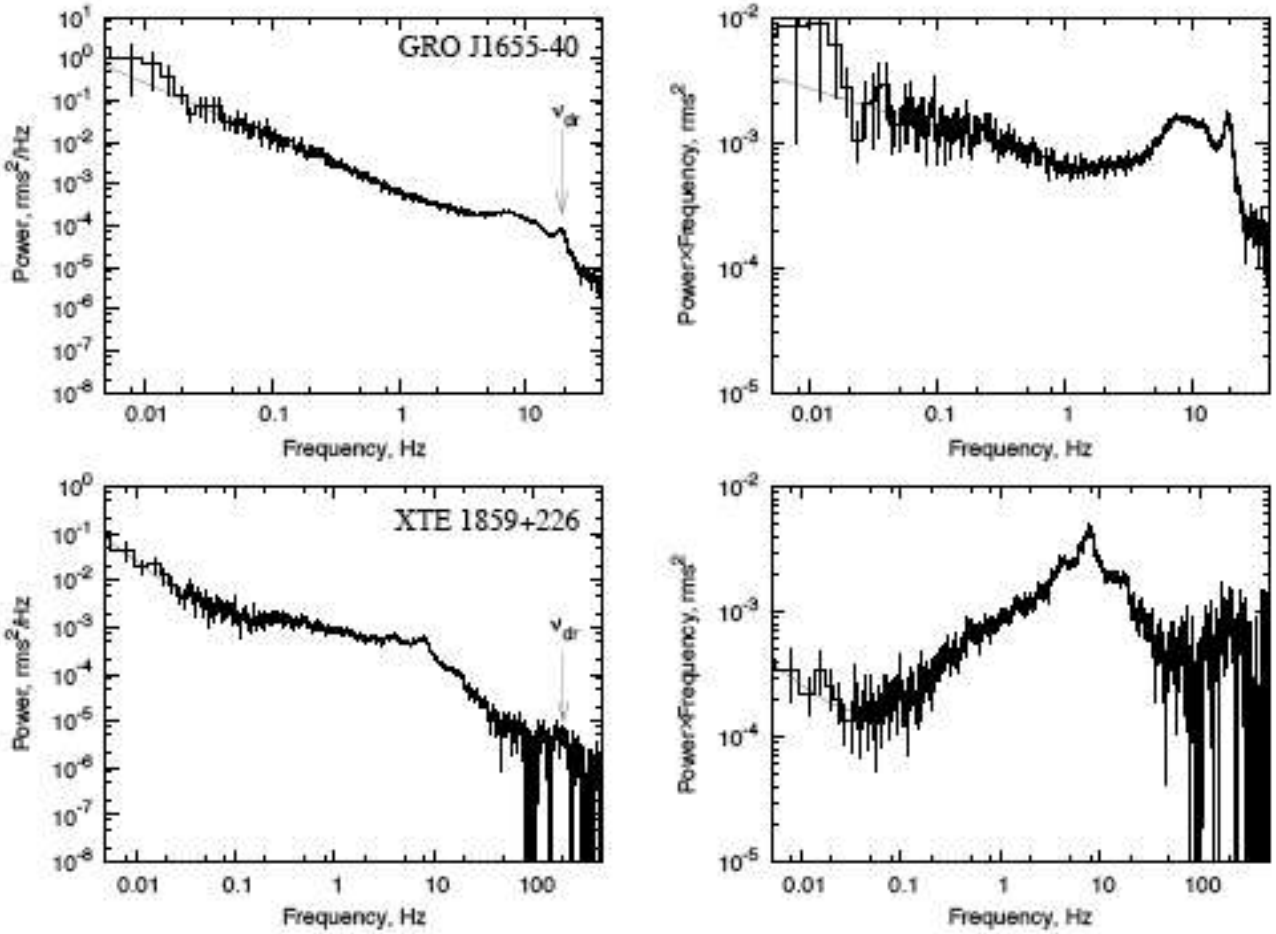

RXTE/PCA power spectra (left panels) and power×frequency diagrams (right panels) of GRO J1655-40 (top) and XTE 1859+226 (bottom). One can clearly see QPO frequencies dr at 10 – 20 Hz for GRO J1655-40 and 185 Hz for XTE 1859+226 before a high-frequency cut-off. The rms^2 power at ν_{dr} is comparable (GRO J1655-40) or higher (XTE 1859+226) than that at low frequencies (see right panels).

Summary I.

We present a model of Fourier Power Density Spectrum (PDS) formation in accretion powered X-ray binary systems derived from the first principles of the diffusion theory.

The resulting PDS continuum is a sum of two components, a low frequency (LF) component is presumably originated in an extended accretion disk and a high frequency (HF) component is originated in the innermost part of the source (Compton cloud).

Summary II.

The LF PDS component has a power law shape with index about 1.5 at higher frequencies ("red" noise) and a flat spectrum below a characteristic (break) frequency ("white" noise).

This white-red noise (WRN) continuum spectrum holds information about physical parameters of bounded extended medium, diffusion time scale and dependence of viscosity vs radius.

We offer a method to measure an effective Reynolds number, Re using the basic PDS parameters (PDS index and characteristic frequencies).
We obtain that the inferred Re in the range of 8 ± 2.5.

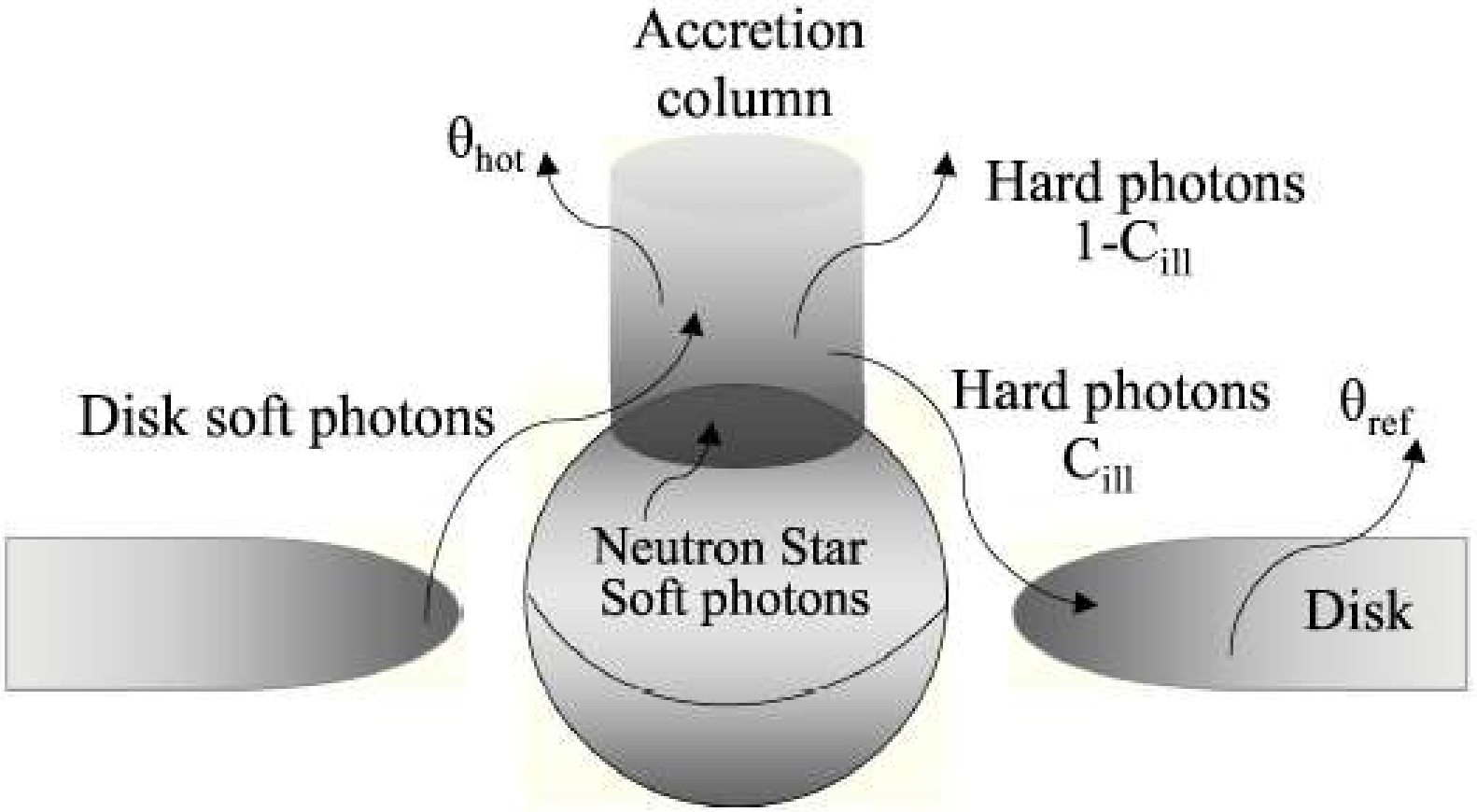

This cartoon illustrates the different emission patterns responsible for the time lags of the pulsed emission. Cill is the disk illumination fraction. Soft time lag of the pulsed emission is the result of downscattering of hard X-ray photons in the relative cold plasma of the disk. A fraction of hard X-ray photons 1- Cill that are upscattered soft disk photons coming from the disk and NS and directly are seen by the Earth Observer.

Time lags and density variations in compact objects

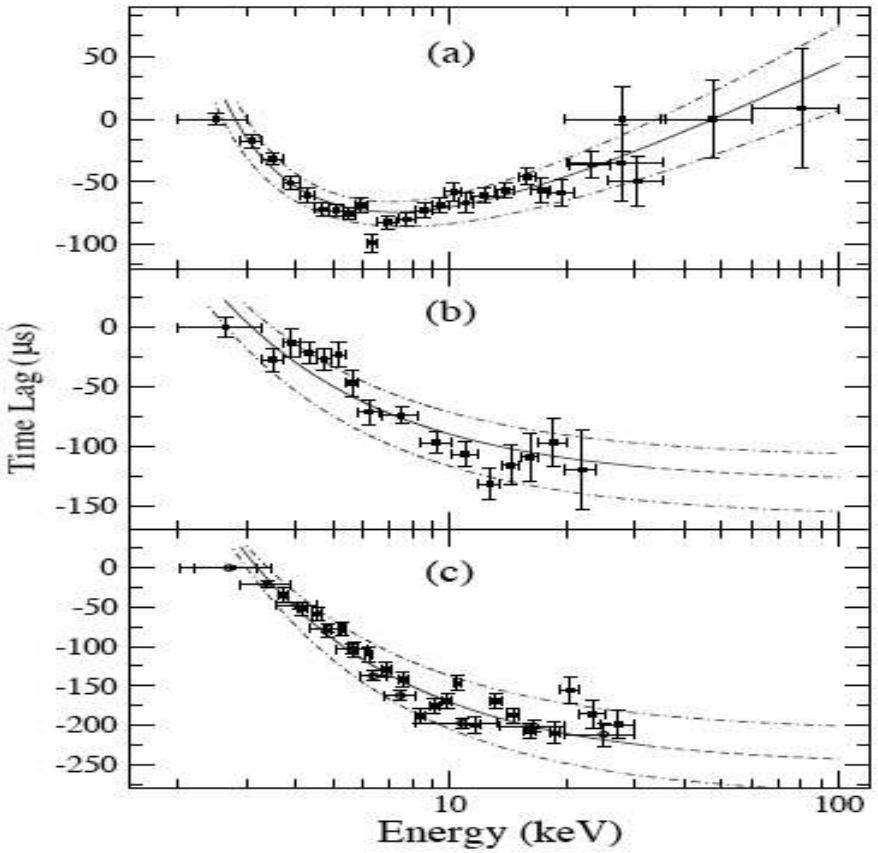

The measured soft time lag of the pulse profile versus energy (crosses) with respect to the first energy channel. The best- fit curve using the Comptonization model is shown with the solid line. The upper and lower limit of the electron number density of the Comptonization emission area, are given in dot-dashed line 1.6-2.6 x 10^{18} cm^{-3} . The panels corresponds (a) for IGR J00291+5934 including also the upper and lower limit of the electron number density of the reflector, 6.1-8 x 10^{18} cm^{-3}, and (b) that for XTE J1751-305, 6-6.6 x 10^{18} cm^{-3} and (c) that for SAX J1808.4-3658, 2.9-3.6 x 10^{18} cm^{-3}.

Time lag model

$$\Delta t = -\frac{C_{\rm ill}}{\sigma_{\rm T} n_{\rm e}^{\rm ref} c} \times$$

$$\left[\frac{1}{4\theta_{\rm ref}} \ln \frac{1 - 4\theta_{\rm ref}/z}{1 - 4\theta_{\rm ref}/z_*} - \frac{n_{\rm e}^{\rm ref}}{n_{\rm e}^{\rm hot}} \frac{1 - C_{\rm ill}}{C_{\rm ill}} \frac{\ln(z/z_*)}{\ln[1 + (3+\alpha)\theta_{\rm hot}]} \right] \quad (5)$$

where $n_{\rm e}^{\rm ref}$ is the electron number density of the reflector, $n_e^{\rm hot}$ is the electron number density of the Comptonization emission area (accretion column). $\theta_{\rm ref} = kT_e^{\rm ref}/(m_e c^2)$ is a dimensionless temperature of the reflector. We assume a typical value of $\theta_{\rm ref} < 0.7$ keV/511 keV. $kT_{\rm e}^{\rm hot}$ and α are the best-fit parameters for the hot plasma temperature and spectral index of the Comptonization spectrum, and $\theta_{\rm hot} = kT_e^{\rm hot}/(m_e c^2)$.

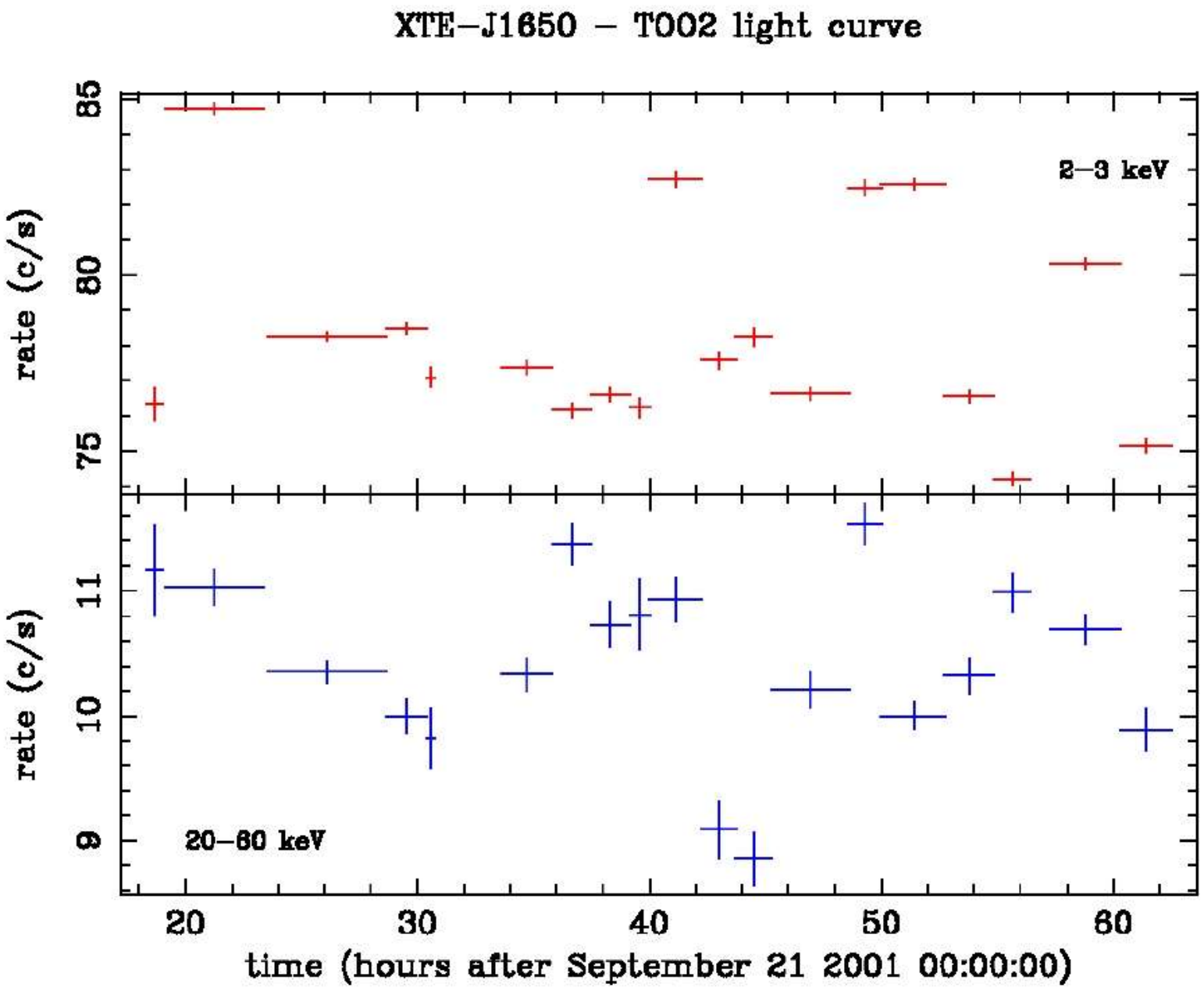
XTE−J1650 − T002 light curve
2−3 keV
20−60 keV
rate (c/s)
rate (c/s)
85
80
75
11
10
9
20
30
40
50
60
time (hours after September 21 2001 00:00:00)

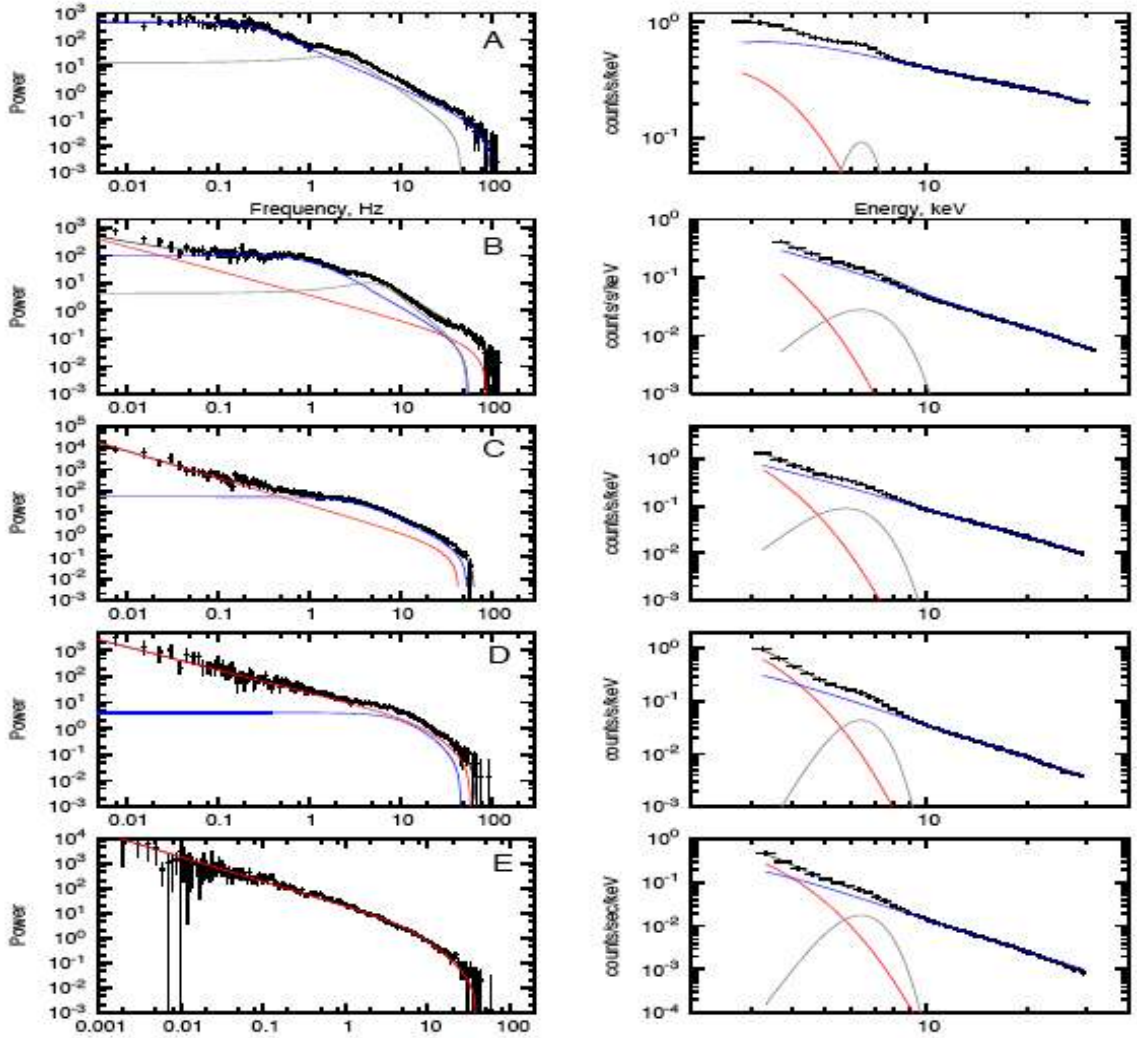

Fig. 2.— Cyg X-1: Observable power spectrum (PDS) (left panel) vs photon spectrum (right panel) from low/hard to soft state of Cyg X-1. Data points are shown with error bars. PDS is fitted by a product of sum of LF and HF white-red noise power spectra and Lorentzian (see formula 67). We also use Lorentzians to fit QPO features. Black line is for the resulting PDS as red and blue lines present LF and HF components respectively. Photon spectrum is fitted by BMC+GAUSSIAN model. Black line is for the resulting spectrum as red and blue lines present BMC blackbody and Comptonization components respectively. Grey line presents GAUSSIAN of K_α line located at 6.4 keV.

W01 demonstrated that the mass accretion rate in the disk $\dot{M}$ *can be calculated as*

$$\dot{M} = 3\pi \frac{\partial V}{\partial x}.$$

Furthermore, we assume that the mass accretion rate at the inner disk edge is converted with efficiency $\varepsilon_{\rm eff}$ *into the X-ray luminosity, L(t) i.e.*

$$L(t) = \varepsilon_{\rm eff} \dot{M}(t, R_{in})$$

and thus

$$X(t) = L(t) \propto \frac{\partial V}{\partial x}(t, 0).$$

Now we consider a general case of problems where $\hat{\nu}(x) = (\hat{\nu}_0 / x_0^{\psi}) x^{\psi}.$

a. Viscosity linearly distributed over radius: $\psi = 2$

$$X(t) \propto \sum_{k=1}^{\infty} \exp[-\pi^2 (2k-1)^2 t / 4t_0]$$

where the viscous time scale $t_0 = 4x_0^4 / 3\hat{\nu}_0 = 4R_0^2 / 3\hat{\nu}(R_0).$

Then the power spectrum of X(t) is:

$$||F_X(\nu)||^2 \propto \sum_{k=0}^{\infty} \frac{1}{(8t_0\nu/\pi)^2 + (2k+1)^4}$$

where $F_X(\omega) = \int_0^{\infty} e^{-i\omega t} X(t) dt$